MINISTRY OF HEALTH OF THE REPUBLIC OF UZBEKISTAN BUKHARA STATE MEDICAL INSTITUTE

Radjabov Akhtam Boltaevich Rasulova Mokhigul Matyokub kizi

AGE-RELATED MACROANATOMY OF THE PROSTATE GLAND, ITS RELATIONSHIP WITH INDICATORS OF PHYSICAL DEVELOPMENT AND STRUCTURAL CHANGES IN CHRONIC ALCOHOLISM

(Monograph)

В монографии В комплексной форме изложены результаты исследования, посвящённого особенностям формирования и динамики изменений биометрических характеристик предстательной железы, а также показателей физического развития в различные этапы постнатального онтогенеза и при хронической алкогольной интоксикации. На основе полученных данных детально определены топографическое расположение органа, его морфологические варианты, темпы прироста массы и линейноанатомических параметров, а также выявлены корреляционные взаимосвязи характеристиками. Установлено, указанными возрастная трансформация предстательной железы имеет неоднородный характер, что отражается в изменениях её формы и линейных размеров, обусловленных морфофункциональной спецификой органа в разные возрастные периоды. Проведённый анализ показал наличие положительных слабых и умеренных корреляций между объёмом простаты и антропометрическими показателями физического развития у мужчин всех исследованных возрастных групп.

Монография предназначена для научных исследователей фундаментальной медицины, урологов, наркологов, студентов магистратуры.

Монографияда простата безининг биометрик параметрлари ва жисмоний ривожланиш кўрсаткичларининг постнатал онтогенезда ривожланиш, шаклланиш динамикаси ва сурункали алкоголизмда тадкикот натижалари хакида тўлик маълумот келтирилган. Олинган илмий натижаларга асосланиб, органинг топографик жойлашуви, унинг морфологик шакллари, массасининг ўсиш суръатлари хамда простата безининг анатомик кўрсаткичлари аниклаштирилди, шунингдек, мазкур параметрлар ўртасидаги ўзаро боғликлик белгиланди. Простата безининг ёшга доир кайта тузилиш жараёни нотекис кечиб, унинг шакл ва чизикли ўлчамларидаги ўзгаришлар оркали намоён бўлади. Бу холат турли ёш боскичларида органнинг морфофункционал хусусиятлари билан бевосита боғликдир. Тадкикот натижалари шунни кўрсатадики, эркаклар популяциясининг барча ёш гурухларида простата бези хажми билан жисмоний ривожланишнинг антропометрик

кўрсаткичлари ўртасида ижобий, суст ва ўртача даражадаги корреляцион муносабат мавжуд.

Монография фундаментал тиббиёт илмий тадқиқотчилари, урологлар, наркологлар ва магистратура талабалари учун мўлжалланган.

The monograph provides a comprehensive analysis of research findings concerning the dynamics of development and maturation of biometric parameters of the prostate gland, as well as indicators of physical growth during postnatal ontogenesis and under conditions of chronic alcohol intoxication. The obtained data allowed for a detailed determination of the organ's topography, morphological variations, growth rates of its mass, and anatomical characteristics. Furthermore, statistical analysis revealed correlations between these parameters. It was established that age-related remodeling of the prostate proceeds in a non-uniform manner, manifested through alterations in its morphological and linear dimensions, which are directly linked to the organ's morphofunctional characteristics at different stages of life. The study also demonstrated the presence of positive, weak to moderate correlations across all examined age groups between prostate volume and anthropometric indices of physical development in the male population under investigation.

This monograph is aimed at specialists in fundamental medicine, including urologists, narcologists, and postgraduate researchers.

Macroanatomical characteristics of the prostate gland in relation to age, its relationship with physical development indicators and structural changes in chronic alcoholism[text] / Radjabov Akhtam Boltaevich , Rasulova Mokhigul Matyokub kizi/ Bukhara:

UDC

Authors:

Radjabov A.B. - Head of the Department of Anatomy, Clinical Anatomy(OSTA), DSc.

Rasulova M.M. -assistant of the Department of Anatomy, Clinical Anatomy(OSTA).

Reviewers:

Rasulov H.A. - Head of the Department of Anatomy and Pathological Anatomy of the Tashkent Pediatric Medical Institute, Doctor of Medical Sciences.

DSc, Khamdamova M.T. - Professor of the Department of Obstetrics and Gynecology No. 2 of the Bukhara State Medical Institute.

TABLE OF CONTENTS

INTRODUCTION6
CHAPTER I. MACROANATOMY OF THE PROSTATE GLAND IN
POSTNATAL ONTOGENESIS AND UNDER THE INFLUENCE OF
VARIOUS ENVIRONMENTAL FACTORS 8
1.1-§. Anatomical features of the prostate gland of mammals
1.2-§. Microanatomical characteristics of the mammalian prostate
1.3-§. Anatomy of the prostate gland under the influence of environmental factors
CHAPTER II. DESIGN AND METHODOLOGY OF CONDUCTING A
MACROSCOPIC RESEARCH36
2.1-§. Analysis of the experimental research
2.2-§. Characteristics of the research methods used
CHAPTER III. MACROSCOPIC STRUCTURE OF THE PROSTATE OF
RATS OF THE CONTROL GROUP IN POSTNATAL ONTOGENESIS 43
3.1-§. Macroanatomy of the rat prostate gland in early postnatal ontogenesis 43
3.2-§. Macroanatomical characteristics of the rat prostate in late postnatal
ontogenesis
CHAPTER IV. ANATOMY OF THE PROSTATE GLAND OF RATS OF
THE EXPERIMENTAL GROUP 60
4.1-§. Macroanatomy of the prostate in rats with chronic alcoholism 60
CHAPTER V. ULTRASONIC MORPHOMETRY OF THE HUMAN
PROSTATE DURING POSTNATAL ONTOGENESIS AND DURING
CHRONIC ALCOHOL EXPOSURE 68
5.1-§. Age morphometry of biometric parameters of the human prostate gland
according to ultrasound data
5.2-§. Echographic characteristics of the prostate in men suffering from chronic
alcoholism

CHAPTER V	I. ANTHROPOMETI	RIC CHARACTER	RISTIC	CS OF H	lUMAN
PHYSICAL	DEVELOPMENT	INDICATORS	IN	POST	NATAL
ONTOGENES	SIS AND UNDER CHI	RONIC ALCOHOI	EXP	OSURE	75
6.1-§. Morpho	metric parameters of p	hysical developmen	t of m	nales in p	ostnatal
ontogenesis an	d its relationship with bi	ometric indicators o	f the pi	rostate	75
6.2-§. Morphor	metric characteristics of	physical developme	ent ind	icators in	chronic
alcoholism				• • • • • • • • • • • • • • • • • • • •	80
CONCLUSIO	N	•••••	••••••	•••••	82
LIST OF REF	FERENCES	•••••	•••••	•••••	97

The reproductive function of mammals is fundamental to the perpetuation of life on Earth, making any disturbances in this system capable of producing significant global consequences. Recent reports indicate that men worldwide are exhibiting pronounced declines in sperm quality, with fertility rates decreasing and prenatal mortality becoming more frequent, underscoring the urgent need to investigate the underlying causes of reproductive dysfunction and elucidate their mechanisms (Sayapina I.Yu., 2018; Aboyan I.A. et al., 2020; Lanina V.A. et al., 2020; Magri V. et al., 2019).

A critical review of the current literature on prostate morphology reveals that, although numerous studies exist, most focus on isolated developmental stages of the gland. The comprehensive analysis of the formation and age-related growth of the prostate's anatomical parameters remains largely unexplored (Ustenko R. L., 2013; Gromov A. I. et al., 2017; Petko I. A., Usovich A. K., 2019; Bannowsky A. et al., 2018).

This research aims to establish a foundation for future investigations into the age-dependent structural transformations of the prostate, providing clarity on the sequential stages of its development and informing strategies for the prevention and management of related disorders.

A significant challenge in contemporary medicine is understanding the mechanisms underlying chronic alcoholism. At present, the influence of alcohol on the growth and maturation of the prostate gland remains poorly characterized. Precisely which stage of development is most susceptible to the disproportionately deleterious impact of alcohol on the formation of the prostate's morphological structures remains undetermined—an issue of substantial relevance to both theoretical research and clinical practice. (Rocco A. et al., 2014; Ivanets N.N., 2016). This uncertainty complicates the accurate interpretation of the prostate's functional roles under normal conditions and in pathological states. Investigating this issue would facilitate the identification of the mechanisms by which alcohol damages male reproductive organs.

A synthesis of recent literature (Trufanov G.E., Ryazanov V.V., 2016; Alyaev Yu.G. et al., 2018; Brock M. et al., 2018; Zyryanov A.V. et al., 2020) indicates that available data on ultrasound-based morphometric assessment of the prostate gland are predominantly restricted to isolated findings within narrowly defined age cohorts. In most cases, these measurements are obtained incidentally during diagnostic evaluations for specific pathological conditions, which leads to datasets that are small in volume, fragmented in scope, and insufficiently standardized with respect to physical development indices or age-related variability. At present, there is a notable absence of comprehensive, systematic information on the age-specific ultrasound anatomy of the male prostate across the full span of postnatal ontogenesis. Likewise, the developmental patterns of prostate biometric parameters under chronic alcohol exposure remain poorly characterized. Closing these knowledge gaps would provide a scientific basis for formulating clinical guidelines that link prostate anatomical metrics with chronological age and the influence of environmental chemical factors. Consequently, in the formulation of national reference standards for the morphometric parameters of the prostate at different stages of postnatal development, it is imperative to conduct targeted research on the correlations between the organ's metric characteristics and indicators of physical maturation.

CHAPTER I. MACROANATOMY OF THE PROSTATE GLAND IN POSTNATAL ONTOGENESIS AND UNDER THE INFLUENCE OF VARIOUS ENVIRONMENTAL FACTORS

1.1-§. Anatomical features of the prostate gland of mammals

The male reproductive system in mammals comprises paired testes, the epididymis, and various accessory gonads, with these structures differing in shape and anatomical location [57, 103, 173]. There is considerable interspecies variability in the anatomy, physiology, function, and number of male accessory glands. In

mammals, these accessory glands include the prostate, the coagulating gland (also referred to as the anterior prostate), seminal vesicles, ampullary glands, bulbourethral glands, urethral glands, and preputial glands. While not every accessory gland is present in all species, with the exception of certain transgenic rodents, all of these glands are consistently found in rats and mice [83].

According to several authors [112, 154], accessory sex glands in mammals can be classified into four main types: ampullary, vesicular, prostatic, and bulbourethral glands. The morphological characteristics of these glands—such as number, size, and shape—vary considerably among species, and some glands may be absent entirely in certain mammals. Nonetheless, the prostate is a consistent feature present in all male mammals [81, 116].

Among mammals, rodents display the highest variability in the organization of accessory sex glands. In rats, four anatomically distinct prostatic lobes are present [77], a condition also observed in chinchillas (*Chinchilla lanigera*) [77, 79] and the spotted paca (*Agouti paca*) [70]. Rabbits possess vesicular glands, a well-developed prostate, and small, ventrally positioned bulbourethral glands [63]. The capybara exhibits a full complement of prostatic, vesicular, coagulating, and bulbourethral glands [91], while guinea pigs have coagulating glands, seminal vesicles, bulbourethral glands, and a prostate [156]. In Persian squirrels, the accessory glands are represented by the prostate, bulbourethral, and coagulating glands. Holtz and Foote [101], in their examination of adult male Dutch rabbits, documented vesicular, prostate, prostatic, paraprostatic, and bulbourethral glands as components of the accessory sex gland complex.

In decorative (pet) rabbits, the accessory sex gland complex consists of paired vesicular and bulbourethral glands, the prostate gland, and the vestigial male uterus. [38]. Several authors [95, 105, 120] describe the rodent prostate as having a multilobular structure, consisting of four bilaterally symmetrical lobes that encircle the urethra at the base of the bladder. These lobes are classified as the ventral, lateral, dorsal, and anterior lobes, the latter also known as the coagulating gland, which connects to the seminal vesicles. Contrastingly, Key Pinheiro PFF et al. [107] and

Rochel SS et al. [147] propose an alternative classification dividing the rodent prostate into dorsal, dorsolateral, and ventral lobes.

Rodent prostate lobes are elongated, tubular, and opaque, with their nomenclature reflecting their anatomical positions surrounding the urethra [85]. In other mammals, such as dogs and humans, the prostate does not exhibit a multilobular organization in adulthood. Instead, it has a simpler structure composed of closely interconnected zones that form a compact glandular organ [124, 140].

Although discrete lobes are a common characteristic in most studied rodents, some variations have been documented. In rats and mice, for instance, the lateral and dorsal lobes are frequently merged into a dorsolateral lobe due to their shared ductal origin, anatomical proximity, and a delayed epithelial response to androgen deprivation [105, 157]. By contrast, the ventral lobe in these species is the most prominent component of the prostate complex, demonstrates a faster epithelial reaction to androgen ablation, and serves as the principal experimental model for studying prostate biology [157, 159].

Prostate anatomy differs substantially across mammalian species; however, the gland is generally situated beneath the bladder and anterior to the rectum. Species with relatively large testes tend to possess a highly developed prostate [130].

The rat prostate consists of four distinct pairs of lobes—dorsal, lateral, ventral, and the coagulating (or coiled) gland—classified according to their anatomical relationship to the urethra, into which their ducts open. The dorsal lobe lies beneath and posterior to the junction of the seminal vesicles and coagulating gland, surrounding the urethra dorsally. The lateral lobe is positioned directly below the seminal vesicle and coagulating gland. The ventral lobe arises from the ventral aspect of the urethra, immediately beneath the urinary bladder; it is the largest lobe, comprising approximately half of the total prostatic mass, and is the most easily dissected from the remainder of the gland [54, 67, 83, 95, 99, 111, 130, 160, 161]. Owing to the difficulty in differentiating the dorsal and lateral lobes [152] and their close histological resemblance [171], they are frequently classified together as the dorsolateral prostate. The coagulating gland—also termed the dorsocranial or

anterior prostatic gland due to its morphological similarity to the prostate—is attached to the lesser curvature of the seminal vesicles [68, 69, 83, 99, 110], a close association not observed in humans. The prostatic lobes extend into the abdominal cavity, with their ducts delivering secretions into the urethra during ejaculation [132]. Interestingly, Nozdrachev A.D. and Polyakov E.L. [33] regard the rat prostate as bilobed.

In the brown rat, the prostate is divided into dorsal and ventral regions, both of which are large and well developed. The irregularly shaped dorsal region lies beneath the seminal vesicles and adjoins the posterior aspect of the urethra, while the ventral region surrounds the initial segment of the urethra and comprises two lateral lobes [28].

According to Savelieva A.Yu. [38], in decorative rats, the prostate is relatively small, bilobed, and envelops the initial portion of the vas deferens. It runs parallel to the lateral urethral wall, opening into the urethra through numerous excretory ducts.

Research by Adebayo A. et al. [58] demonstrated that the large cane rat's prostate is brown and consists of paired lobes positioned at the sides of the bladder neck. The right lobe comprises four distinct lobes—cranial, dorsal, lateral, and ventral—whereas the left lobe consists of three less distinct lobes: dorsal, lateral, and ventral.

The macroscopic lobulation of the cane rat prostate is notable for its similarity to the prostate of other species such as rats [99], gerbils [80], chinchillas [79], dogs [131], and cats [174]. These glands are paired and lobed, yet they do not entirely encircle the pelvic urethra, contrasting with rats, which possess two lateral, dorsal, and ventral lobes, or other species with two undivided lobes.

The mouse prostate closely resembles that of the rat, comprising four lobes with a comparable anatomical arrangement. In contrast to the human prostate, which is anchored to the base of the bladder and rectum, all lobes of the mouse prostate are freely suspended within the pelvic cavity [84, 85, 134, 168]. These findings align

with the results reported by other researchers [98, 102, 110, 162], who observed similar prostatic structures in mice.

In jumping mice, the prostatic complex is represented exclusively by the ventral lobe [166]. In the gerbil (*Gerbillus tarabuli*), the prostate is organized into four paired lobes—ventral, dorsolateral, dorsal (encircling the prostatic segment of the urethra), and an anterior lobe situated along the concave surface of the seminal vesicles [108]. A comparable lobar arrangement has been documented in Mongolian gerbils (*Meriones unguiculatus*) [147]. In guinea pigs, the prostate encircles the urethra and is located immediately caudal to the bladder neck, caudomedial to the coagulating gland, and lateral to the seminal vesicles. It is composed of two lobes—a large, well-developed dorsal lobe and a smaller ventral lobe—linked by a transverse isthmus. On the right side, the prostate and coagulating gland form a single anatomical complex without a shared capsule [156]. Similar observations were reported by Mukhotrofimova O.M. [28] in guinea pigs, although the lobes were designated as cranial and caudal rather than dorsal and ventral.

In ferrets, the prostate constitutes the only accessory sex gland, forming a complete ring around the base of the urethra adjacent to the bladder neck [38, 104]. Structurally, it consists of dorsal and ventral portions and is topographically positioned at the transition between the abdominal and pelvic cavities, entirely encircling the urethra [139].

In the golden hamster, the prostate is divided into two structurally distinct components. The ventral portion, located at the proximal segment of the urethra near the bladder, is formed by convoluted tubular structures. The larger dorsal portion has a triangular configuration and consists of elongated, tortuous tubules positioned adjacent to the posterior aspect of the urethra, directly beneath the rectum [28].

In African striped ground squirrels, the prostate is a single, spherical gland located immediately below the urinary bladder [113]. In Persian squirrels, the prostate is uniquely heart-shaped, dense, and smooth, positioned compactly in the dorsal region of the pelvic urethra [60].

Research findings indicate that in the agouti, the prostate gland is differentiated into dorsal and ventral portions [126]. In capybaras [126] and chinchillas [79], however, the prostate is organized into three approximately equal lobes, comprising two lateral and one medial lobe.

Descriptions of the rabbit prostate are among the most debated in the literature. It is reported to consist of three segments: the proprostate, the prostate proper, and the paraprostate [101, 122]. The proprostate is positioned posterior to the vesicular gland and anterior to the principal prostate. In contrast, both the prostate and the paraprostate are located rostral to the bulbourethral glands. These anatomical components discharge into the pelvic urethra bilaterally, adjacent to the seminal tubercles [167].

In decorative rabbits, the prostate encircles the urethra in the cervical region, is closely associated with the male uterus, and is composed of five lobes [38].

Telenkov V.N. [42], in studies of the prostate glands of fur-bearing animals, found that in arctic foxes and red foxes, the prostate consists of two bean-shaped lobes located at the beginning of the urogenital canal. In sables and minks, the gland comprises two ellipsoid lobes positioned in the middle of the urogenital canal.

Further investigations of the pelvic organs in predators and lagomorphs by Telenkov V.N. [43] demonstrated that the prostate is situated along the anterior and lateral walls of the urogenital canal, closely enveloping its prostatic portion. The lobes extend toward the neck of the urinary bladder, consistent with findings on the vesicoprostatic complex in minks [10] and silver foxes [4].

In dogs, the prostate is the sole male accessory gland and presents as a bilobed, oval structure within the pelvic cavity [92]. Similar observations were reported by LeRoy and Northrup N. [115], who described the organ as an ovoid, two-lobed gland. Evans H.E. and de Lahunta A. [89] noted that the gland's size and weight vary with age, breed, and body mass. They reported that the prostate is semi-oval in cross-section, with a flattened dorsal surface. In puppies younger than two months, the prostate gland is situated within the caudal portion of the abdominal cavity. As the animal approaches sexual maturity, it migrates into the pelvic cavity. After the

attainment of sexual maturity, the organ undergoes cranial enlargement, with a portion projecting into the abdominal cavity[89, 155].

In rabbits, the prostate consists solely of a dense wall portion, lacking a diffuse component. This wall portion is large, yellowish, and rounded, with a medial groove dividing it into two lateral lobes [30].

In cats, the prostate is bilobed and situated along the posterior wall of the urethra, opening into it through multiple excretory ducts [30].

In the adult European hedgehog, the prostate is a yellow, oval-shaped gland with distinct right and left lobes. The right lobe is larger than the left and is further subdivided into caudal and cranial portions, with the cranial part slightly exceeding the caudal in size. These glands are positioned between the testes, ventral to the urethra and seminal vesicles. On average, the left lobe contains 12 subdivisions, while the right lobe has 13 [59].

In the greater horseshoe bat (*Rhinolophus ferrumequinum*), the prostate is a single, round gland encircling the urethra. It lies dorsodistal to the ampullar-vesicular gland complex, which surrounds the urethra and continues into the urethral gland [106].

In bats such as *Artibeus lituratus*, *Noctilio albiventris* (Noctilionidae), and *Rhynchonycteris naso* (Emballonuridae), as well as in three species of the genus *Sturnira*, the prostate exhibits clearly defined ventral and dorsal regions, each possessing distinct structural characteristics [121, 128, 143].

In three species of Phyllostomidae bats, the prostate is divided into three well-delineated regions: ventral, dorsolateral, and dorsal [90].

According to Moura F. and colleagues [129], in the giant anteater, the prostate gland is situated within the abdominal cavity, positioned dorsally to the urinary bladder and ventrally to the rectum. Based on gross anatomical examination, the authors proposed categorizing the gland into two distinct structural regions: the central zone and the peripheral zone.

In domestic animals, the prostate gland is comprised of a compact (parietal) part and a diffuse part. The compact portion is situated at the neck of the bladder and

includes the right and left lobes along with the isthmus of the prostate. The diffuse portion is embedded within the spongy tissue of the pelvic urethra [30].

In farm animals such as bulls, rams, pigs, and stallions, the prostate is an unpaired gland that partially or largely surrounds the pelvic urethra. It comprises various arrangements of compact and diffuse components, running along the pelvic urethra beneath the urethral muscle. Multiple prostatic ducts open individually on each side into the urethral lumen [93, 146].

In stallions, the prostate consists of two distinct parts. The pars mucosa forms a clasp above the bladder neck and includes the right and left lobes as well as the isthmus. The smaller diffuse portion, along with its glandular elements, lies along the dorsal wall of the urethra [30]. In boars, the prostate functions as a single glandular unit in which the body and diffuse parts are integrated both structurally and functionally [51].

In bulls, the prostate is the sole accessory gland, composed of small lobules embedded within the urethral wall, where the diffuse portion is more fully developed both structurally and functionally [51]. Budras K.D. et al. [73] note that in cattle, the body of the prostate lies on the dorsal surface of the urethral between the vesicular glands and the urethral muscle. The extended portion of the prostate measures approximately 12–14 cm, is concealed within the urethral wall, and is covered anteriorly and laterally by the urethral muscle.

In rams, the diffuse portion of the prostate is situated along the dorsal wall of the urethra, with the parietal (compact) component absent [30]. In Barka goats (*Capra hircus*), the sole prostate is positioned near the entry of the vesicular gland into the pelvic region and consists exclusively of the diffuse part, which is encapsulated by connective tissue [61]. Comparable findings have been reported in Indian goats (Kundu P. [114]) and pampas deer (Perez W. et al. [138]). Gofur M. [97] observed that in black Bengal deer, the single prostate comprises two components: a compact (external) and a diffuse (internal) part. Additionally, Pathak A. et al. [137] noted that some Gaddi goats possess an extra segment termed the prostate body.

In humans, the prostate is a pyramid-shaped organ located beneath the urinary bladder, with its apex in contact with the prostatic urethra and its base adjacent to the bladder [136]. It lies anterior to the rectum and encircles the prostatic urethra, which serves as the conduit for urine from the bladder. The normal prostate typically weighs between 15 and 20 grams [102].

Beyond secreting a specialized fluid with barrier properties, the prostate works in conjunction with the detrusor muscle of the bladder to function as a sphincter, regulating urination [100, 144, 150]. In males, the prostate is a walnut-sized, tubuloalveolar gland located beneath the bladder [117, 164], anatomically divided into the base, middle portion containing the seminal tubercle, and the apex [65].

In adult men, the prostate can assume three distinct shapes: dome-shaped, cone-shaped, and wedge-shaped. In younger men and those in early middle age, the cone-shaped configuration predominates, whereas in later middle age and older individuals, the dome-shaped form is more common. Morphometric parameters of the prostate, including size and mass, are influenced by its shape, with both increasing in elderly and senile men [45].

Marked morphological distinctions are observed between the prostate gland of adult humans and that of rodents. In rodents, the prostate demonstrates a lobular configuration, consisting of paired anterior, ventral, and dorsolateral lobes—structures absent in the human counterpart. In humans, the gland is enclosed within a compact fibromuscular capsule and embedded in a dense stromal framework, whereas in rodents, it is surrounded by only a delicate stromal sheath [87]. In contrast to the lobular arrangement of rodents, the human prostate is organized into functional zones—central, transitional, and peripheral—each encompassed by a sturdy fibromuscular capsule. The precise anatomical equivalence between murine prostatic lobes and the zonal architecture of the human prostate remains a subject of scientific discussion and ongoing investigation [85].

The human prostate is composed of compact, non-homologous zones, prompting questions about which segments of the rodent prostate most accurately correspond to the human gland. Multiple studies have indicated that there is no direct correlation between the sizes of human and rodent prostates [72, 165].

Unlike in rodents, the human prostate fully encircles the urethra and lacks external lobular divisions. It contains distinct histologically defined regions: the peripheral zone, central zone, transition zone, and the non-glandular anterior fibromuscular region [123]. The peripheral zone surrounds the proximal portion of the prostatic urethra. Based on anatomical [141]and interspecies immunohistochemical studies [64], the dorsolateral lobe of the mouse is considered homologous to the human peripheral zone, which is the site of approximately 80% of human prostate adenocarcinomas [86, 133].

The central zone, analogous to the mouse anteroposterior lobe, is a cone-shaped region surrounding the vas deferens and accounts for roughly 25% of the prostate volume. The transition zone, the smallest region comprising 5–10% of the prostate, surrounds the distal prostatic urethra [66]. Roy-Burman P. et al. [149] noted that this zone lacks a direct murine homologue and is the primary site of benign prostatic hyperplasia in humans [86]. Therefore, while the human urethra is fully enveloped by the prostate, this configuration is not observed in rodents.

In males prior to the onset of puberty, the prostate gland has an approximate mass of 2 grams. With the increase in circulating androgens during pubertal development, the organ undergoes significant enlargement, attaining an average weight of nearly 20 grams in healthy adult men. This size generally remains stable until roughly the fifth decade of life, after which the prevalence of benign prostatic hyperplasia begins to increase noticeably [169].

The shape and internal structure of the prostate also change with age. Until about 11–12 years, the gland is nearly spherical, gradually assuming a horse chestnut-like form. By 16–17 years, the division into right and left lobes, as well as base and apex, begins, with the middle lobe becoming anatomically distinct only between 20 and 22 years of age [34].

In summary, a key distinction in prostate orientation between animals and humans lies in its directional alignment: it is horizontally positioned in most animals, following the orientation of the body, whereas in humans it is vertically oriented. The prostate also exhibits species-specific structural characteristics. In rodents and many other mammals, the gland displays a multilobed organization, while in humans and dogs, it is a single, compact organ with a simpler architecture.

1.2-§. Microanatomical characteristics of the mammalian prostate

The prostate gland in mammals is a highly specialized tubuloalveolar exocrine organ [32, 82, 89, 90, 91, 106].

In rats, each prostatic lobe is surrounded by a delicate capsule of connective tissue. Every lobe consists of numerous secretory units—acini or alveoli—linked to a ramified ductal network, with each lobe discharging its secretions independently into the urethra. The acinar structures are partitioned by loose connective tissue containing stromal cell populations, bundles of smooth muscle fibers, vascular elements, and neural components. The epithelial lining of both acini and ducts includes luminal secretory cells, basal non-secretory cells, and a minor subset of neuroendocrine cells 92, 123, 138]. [73,The luminal cells display a spectrum of morphologies, ranging from cuboidal to tall columnar forms, with cell height modulated by the gland's functional activity and the extent of luminal distension [63, 92, 115, 138]. Encircling each acinus, smooth muscle fibers facilitate the release of prostatic fluid through contraction, producing secretions that exhibit slight eosinophilia—an attribute influenced by protein concentration and the secretory state of the respective lobe [63].

In the cane rat, two histologically distinct lobular types correspond to different anatomical zones of the prostate. The central zone, located near the pelvic urethra, features lobules with nearly round outlines, numerous epithelial folds partially occluding the lumen, and abundant surrounding fibromuscular tissue. The peripheral zone, situated farther from the urethra, contains lobules with wider lumens and comparatively less fibromuscular tissue [42].

In mice, the epithelium lining all prostatic lobes is composed of secretory epithelial cells, basal cells with minimal cytoplasm located beneath the secretory layer, and a small population of neuroendocrine cells, similar to the human prostate. Each lobe is enclosed by a delicate mesothelial covering that incorporates adipose tissue, vascular structures, and neural filaments [89], in agreement with observations documented by D. Oliveira and collaborators [110]. In mice, every prostatic lobe is arranged into discrete tubuloalveolar secretory units connected to a ramifying ductal system, with each duct delivering its contents separately into the urethral lumen. The secretory acini are demarcated from one another by a fibromuscular stromal framework [92, 138]. Similar to humans, the mouse prostate contains epithelial cell types including columnar luminal secretory cells, basal cells, and neuroendocrine cells [121].

A major histological distinction between human and mouse prostates lies in the stromal component. In humans, the anterior fibromuscular stroma is well-developed, whereas in mice, the stroma is sparse with relatively few smooth muscle cells [129].

In other species, epithelial characteristics vary: the agouti prostate exhibits pseudocolumnar epithelium [105], whereas the guinea pig's prostate has simple columnar epithelium [60]. In the Tarabula gerbil, the prostate consists of a folded mucosa with secretory epithelial cells forming tubular units, surrounded by a thin fibromuscular stroma composed of a subepithelial layer and smooth muscle encasing the tubules [91].

In the Mongolian gerbil, all lobes except the dorsal lobe display tubular organization with variable ductal branching, while the dorsal lobe exhibits a tubular-acinar arrangement [120]. These observations differ from the results of Campos SGP

et al. [57], who reported that under morphologically and functionally normal conditions, the central lobe of the Mongolian gerbil prostate consists of tubuloacinar structures lined by simple epithelium and encased by fibromuscular stroma.

In the opinion of Rochel SS et al.[120]dThe dorsolateral and ventral lobes have similar relative volumes between the epithelial and stromal compartments, together occupying approximately 40% of the entire organ. This result indicates that these lobes represent a closer resemblance to the peripheral zone of the human prostate gland, in accordance with the zonal model of ductal architecture described by McNeal[101], whose stromal and epithelial structures occupy approximately half of the gland.

U giant Histologically, the prostate capsule consists of loose connective tissue, blood vessels, nerve ganglia, and muscle bundles. In the central zone, fibromuscular stroma is visualized, filled with epithelial cells of the prostatic duct and urethra with transitional epithelium. In the peripheral zone, there is stromal-fibrous connective tissue with fibroblasts, arterioles, and venules adjacent to the acini, which consist of pseudo-stratified columnar epithelium. In the peripheral zone, young anteaters had 50% fewer acini and ducts of the prostate gland than adults. Interestingly, the prostate gland of the giant anteater has a continuous basal cell layer, similar to that of humans[106].

It is noteworthy that the prostate stroma in giant anteaters contains striated muscle bundles, whereas in most mammals, the gland is composed predominantly of smooth muscle fibers. The presence of striated muscle in the central zone supports the hypothesis that the prostate may exert autonomous control over ejaculation, a feature also observed in humans and dogs [100].

Akmal Yusrizal [43], after examining the male pangolin's accessory sex glands, concluded that the prostate exhibits a lobular organization, with thick connective tissue separating the lobes and lobules, and that the acinar cells are of a mucous type.

In arctic foxes and red foxes, the prostate capsule is relatively thin and primarily composed of connective tissue fibers. In contrast, minks and sables possess a thicker capsule dominated by smooth muscle fibers. The parenchyma in fur-bearing animals displays a tubular-alveolar architecture. Acinar size varies among species, being smaller in arctic foxes and red foxes and larger in sables and minks. Epithelial thickness in the secretory regions is greatest in minks, intermediate in arctic foxes and foxes, and smallest in sables [31].

Within carnivores, the relationship between epithelial and stromal components of the prostate exhibits only minor variation. This structural correspondence between glandular and non-glandular elements is influenced by reproductive seasonality and the absence of bulbourethral glands and seminal vesicles [32].

The rabbit prostate is the most developed among all accessory sex glands, a feature attributed to their continuous, year-round reproductive activity, which necessitates sustained functionality of the sex glands. Despite this, the glandular tissue occupies a relatively small area, explained by the predominance of well-developed muscular tissue within the stromal components of the organ [32].

Several studies report that the capsule of the vesicoprostatic complex in rabbits is primarily composed of smooth and striated muscle fibers, with only a thin layer of elastic fibers interposed and minimal collagen fiber bundles present [67, 145].

In canids, the prostate capsule is thin and mainly consists of elastic and collagen fibers, with a very limited number of smooth muscle fibers organized in bundles. A similar capsule structure has been documented in foxes by Batueva A. B. [4]. By contrast, in mustelids, the capsule is more robust, consisting predominantly of smooth muscle bundles interspersed with collagen fibers, while elastic fibers are arranged superficially in circular and transverse orientations [32].

Randazzo M. and Grobholz R. [116] demonstrated that in canids, septa are composed of smooth myocytes with a minor collagen component, whereas elastic fibers are mainly found in the septa of intermediate and internal lobes. In mustelids, although septa contain few myocytes, this deficiency is functionally compensated by well-developed capsular myocyte layers, as confirmed by Zadonskaya V. Yu. [10].

Badluev E. B. [3] noted that the histological architecture of the septa within the submucosa of the prostate portion of the urogenital canal in rabbits differs from that of predatory species. Both submucosa and septa exhibit smooth muscle fibers with elastic fiber layers, while collagen fibers are nearly absent in the stromal tissue.

Stefanov M., Martín-Alguacil N., and Martín-Orti R. [126] reported that in the secretory regions of the prostate parenchyma of carnivores and lagomorphs, lobules can be classified into primary, intermediate, and internal groups.

The histological findings of Telenkova V.N. [32] regarding the vesicoprostatic complex in carnivores and lagomorphs align with earlier studies [3, 59, 67] describing the tubuloalveolar structure of the prostate in humans and other mammals.

In these animals, the acini of the prostate are lined by a simple columnar epithelium, the height of which ranges from low to tall depending on the degree of luminal distension with glandular secretions. Similar observations have been reported in humans and other mammals [44, 109, 122], including studies of foxes (Batueva A. B. [6]) and rabbits (Badluev E. B. [3]).

In canids, the excretory ducts of the prostate are lined with a multi-row (two to four layers) columnar epithelium, whereas in mustelids the epithelium may contain up to five layers, and in hares, it ranges from one to four layers. Depending on glandular activity and luminal distension, the epithelium may flatten into a single low layer, as reported in studies of various mammals [10, 34, 37, 119, 125].

Fabiane F.M. et al. [72] investigated the prostate morphology in three species of Phyllostomid bats and found region-specific epithelial variations: the ventral region exhibited atypical epithelium lacking clear cellular boundaries; the dorsolateral region displayed pseudostratified cuboidal epithelium in *Carollia perspicillata* and *Phyllostomus discolor*, while in *Glossophaga soricina*, it was columnar; the dorsal region in all three species consisted of pseudostratified columnar epithelium.

In *Artibeus lituratus*, each region of the prostate gland exhibits distinctive structural characteristics. The ventral region possesses an epithelium with variable

morphology due to its holocrine mode of secretion, whereas the dorsal region features a typical pseudostratified cuboidal-columnar epithelium [117].

In the greater horseshoe bat, the prostate is lined with pseudostratified columnar epithelium, which can be classified as transitional epithelium [90].

Histologically, the prostate in three species of bats from the genus *Sturnira* is divided into ventral and dorsal regions. The dorsal region contains tubuloalveolar glands, while the ventral region comprises alveolar glands. The glandular morphology in these species resembles that observed in other members of Stenodermatinae and Desmodontinae, but differs from other subfamilies of Phyllostomidae (Carolinae, Glossophaginae, and Phyllostominae), as well as from species in Molossidae and Vespertilionidae [59].

The canine prostate is morphologically homogeneous and lacks the zonal differentiation observed in the human prostate. It primarily consists of secretory glandular tissue, with stromal projections subdividing the gland into lobules of epithelial tissue. The epithelium is mainly columnar, though it becomes cuboidal within the ducts. Additionally, the prostatic portion of the urethra may exhibit cuboidal, simple columnar, or stratified epithelium [93].

In dogs, the lobules are composed of numerous complex tubular-alveolar glands lined with columnar epithelium [71].

Morphologically, the canine prostate lacks zonal differentiation and exhibits a homogeneous parenchyma along its longitudinal axis [77]. In newborn puppies, a series of elongated main ducts radiate from the prostatic portion of the urethra toward the gland periphery; some of these ducts are luminal, while others are solid [94].

In prepubertal dogs, the prostate is lobular, composed primarily of dense epithelial aggregates without lumina, embedded in a thick stromal framework. Following puberty, androgenic stimulation transforms much of the stromal tissue into prostatic epithelium [95]. The canine prostate typically contains 15 lobules of glandular secretory tissue separated by stromal projections, known as capsular

trabeculae. The majority of the gland is made up of secretory tissue lined by columnar epithelium [76, 134].

As in humans, the normal canine prostate epithelium comprises three cell types: basal, secretory, and neuroendocrine. The secretory cells, either cuboidal or columnar, constitute the bulk of the epithelial population, forming linear tubuloalveolar glands within lobules that empty into small ducts surrounding the urethra [88, 127].

In domestic animals, the prostate parenchyma consists of tubuloalveolar glands lined with simple columnar or cuboidal epithelium. The stroma, constituting roughly one-quarter of the gland, contains abundant vessels and connective tissue fibers [20]. In boars, the secretory portions of the prostate are organized into multiple lobules separated by connective tissue layers, with excretory ducts forming complex folds. The acini are lined with pseudostratified epithelium composed of basal and columnar cells, while the ductal epithelium is shorter than that of the secretory regions. In bulls, the prostate parenchyma is divided into secretory alveoli and excretory ducts of varying sizes and structures; the ducts are lined with pseudostratified epithelium with basal cells interspersed among columnar cells, and the secretory alveoli are lined with simple epithelium of variable height [37].

Mahmud Muhammad Abdullahi et al. [96], after examining the accessory gonads of dromedaries, rams, and Sokoto red bulls, concluded that the dromedary prostate contains the highest proportion of interstitial connective tissue and is particularly rich in striated muscle surrounding the lobules. Fibromuscular trabeculae extend into the parenchyma and are more prominent in dromedaries compared to the other two species. Conversely, Sokoto red bulls exhibited a greater number of secretory acini than the dromedaries and rams.

In all male Bengal goats, the prostate is represented solely by the disseminated portion, located within the submucosa of the dorsal wall of the pelvic urethra. The secretory units and intraglandular ducts are lined with simple cuboidal or columnar epithelium [84]. Similarly, the prostate of the Barka goat (Capra hircus) is encased by a connective tissue capsule, which is thin dorsally and ventrally but thick

laterally. This capsule is covered by a layer of smooth muscle, consistent with reports by other authors [45, 84, 113]. The prostatic acini are lined with simple cuboidal epithelium.

The human prostate is a single gland with distinct histological zones: peripheral, transitional, and central. The peripheral zone comprises approximately 70% of the normal prostate tissue [112, 137]. The transition zone, located around the prostatic urethra, is inconspicuous in most young men and constitutes roughly 5% of the gland. The central zone is cone-shaped, with a broad base at the prostate and an apex at the level of the spermatic cord, surrounding the ejaculatory ducts [47]. Histologically, the human prostate consists of epithelial and stromal components. The epithelium contains three cell types: cuboidal to columnar secretory cells, non-secretory basal cells along the basement membrane, and occasional neuroendocrine cells [81, 130].

The epithelial-to-stromal ratio varies considerably among species. In humans and other primates, the number of cells in the epithelial and stromal compartments is roughly equal, whereas in the adult rat prostate, the ratio is approximately 5:1 [64]. These findings align with the results of Randazzo and Grobholz [116], who reported a roughly equal proportion of stroma and parenchyma in the human prostate.

The cellular architecture of the prostate exhibits notable interspecies variation between humans and rodents. In humans, the proportion of basal to luminal epithelial cells is approximately 1:1, whereas in rodents this ratio is closer to 1:7 [69]. Moreover, human prostates possess a larger volume and higher density of stromal tissue compared with those of rodents [135]. Basal epithelial cells, located adjacent to the basement membrane, display specific differentiation markers that clearly distinguish them from the luminal secretory cell population [66]. In the human prostate, these basal cells form an uninterrupted layer directly beneath the luminal epithelium.

The relatively greater abundance of basal epithelial cells within the human prostate is believed to bear functional relevance. Although their involvement in carcinogenic processes remains a subject of scientific debate, available evidence suggests that depletion of these cells represents an early event in the progression of prostate malignancies in both humans and rats [140]. Furthermore, basal epithelial cells in humans are hypothesized to play a regulatory—or potentially inhibitory—role in the proliferation of prostatic cancer cells [103].

The prostatic stroma is fibromuscular, comprising numerous smooth muscle cells interspersed with fibroblasts, blood vessels, and nerves. In rats, the smooth muscle layer appears to mediate signaling between the mesenchyme and epithelium, contributing to the regulatory mechanisms underlying prostate development [133]. In humans, the prostate is a heterogeneous organ composed of approximately 70% glandular tissue and 30% fibromuscular stroma, enclosed within a thick fibrous capsule [97]. In newborn boys, the prostate already exhibits a complex structure and is functionally comparable to that of an adult [8]. The reduction in acinar area and epithelial height observed in the neonatal prostate likely reflects a decrease in androgen levels during the postpartum period, as suggested by Petko and Usovich [24, 28].

The first significant wave of secretory activity occurs around 13 years of age. By 20 years, the prostate of young men is fully functional. During early adulthood (22–35 years), the gland maintains maximal functional activity. Beyond this period, involutional changes begin, leading to a gradual decline in the number of active acini, possibly due to stagnation of prostatic secretions and the formation of concretions.

Before puberty, the prostate is small and predominantly composed of connective tissue, with stroma between secretory sections formed primarily by smooth muscle fibers. Slow development of the gland occurs between ages 4 and 10. Glandular and non-glandular structures reach maximal development at puberty (16–20 years). From 20 to 35 years, the gland achieves its peak morphofunctional maturity, with well-developed glandular, muscular, and elastic components. After 40 years, the number of functional acini gradually declines, and ongoing transformations in later life result in fibrosis due to involutional processes within the prostate [9].

1.3-§. Anatomy of the prostate gland under the influence of environmental factors

Every individual is continuously exposed to environmental factors, as humans cannot exist independently of their surroundings; these factors are interrelated and exert a reciprocal influence. It is estimated that approximately 85% of all contemporary diseases are linked to adverse environmental conditions resulting from daily and industrial human activities. Environmental influences play a significant role in the development of reproductive dysfunctions [5, 32, 53, 78, 88, 175].

Given the high prevalence of prostate pathology, morphofunctional changes in the organ induced by environmental factors warrant particular attention [125, 163]. Zakharov A.A. [13] reported that in immature rats, exposure to the immunosuppressant cyclophosphamide led to a decrease in prostate mass, reductions in volumetric and linear parameters, and flattening of the epithelial lining of the acini. Similarly, Kashchenko S.A. and Zakharov A.A. [19] observed in aged rats subjected to cyclophosphamide-induced immunosuppression a statistically significant decrease in both absolute and relative organ mass, alterations in micromorphometric parameters of epithelial cells in the secretory regions, and significant deviations in linear and volumetric measurements of the prostate.

In experimental rats exposed to subzero temperatures, the prostate exhibits pronounced structural and functional alterations, characterized by enhanced proliferative and secretory activity of the acinar epithelium. The gland demonstrates congestive changes, including venous stasis and expansion of the acinar lumens, accompanied by focal epithelial hyperplasia, diffuse proliferation of connective tissue, and lymphocytic infiltration of the stroma [39].

Hypokinetic stress induces microcirculatory disturbances within the prostate vasculature of rats. Prolonged sedentary conditions lead to compensatory

enlargement of vessel areas, promoting restoration of hemocirculation through vascular dilation and angiogenesis [26].

In rats with experimentally induced prostatitis, histological examination revealed diffuse lymphocytic infiltration, stromal edema, and variability in the shape and size of connective tissue end sections. Secretory material was present in approximately 70% of the acini, with focal hemorrhages observed in certain regions [41].

Histological studies in young rats with chronic prostatitis demonstrated leukocyte infiltration of the interlobar stroma, narrowing of acinar lumens, and atrophic changes of the epithelial lining. Accumulation and stagnation of secretions in the glandular sections led to increased acinar size and glandular deformation. Metaplasia of the secretory epithelium, epithelial dystrophy, and pathological proliferation of connective tissue were also noted [46].

In cases of chronic autoimmune prostatitis, the prostate displayed classic morphological signs of chronic inflammation: acinar epithelial atrophy, luminal expansion, diffuse fibrosis of the connective tissue stroma, and lymphocytic infiltration. Morphometric analyses indicated an increased volume fraction of inflammatory infiltrate, a higher proportion of acini lacking secretion, and elevated numbers of epithelial cells within the acinar lumens [50].

Neimark A.I. et al. [31] examined agricultural machine operators with vibration disease and observed a reduction in the number and size of principal cells in prostate biopsies. The acinar lumens appeared predominantly folded, containing desquamated cells and amyloid bodies. Focal epithelial atrophy was detected in some areas, while periacinar fibrosis was observed throughout the tissue.

In rat models of alcohol intoxication, venous congestion in the pelvic organs was accompanied by structural alterations in the prostate, including edema, disorganization of glandular architecture, and vascular dilation. Chronic alcohol exposure led to expanded acinar lumens, accumulation of secretion, increased hemocapillary cross-sectional area, reduced parenchymal volume, and augmented stromal content [56].

Histological studies in mature men (31–40 years) with chronic alcohol intoxication revealed glandular polymorphism, reduced acinar diameter and number, decreased epithelial height, and diminished glandular tissue fraction. Conversely, the proportion of muscular and connective tissue increased, occasional lymphoid infiltrates were present in the stroma, and arterial walls showed significant thickening due to sclerosis [6].

Favaro W.J. and Cagnon V.H.A. [93] in 45-day-old rats, and Candido E.M. et al. [78] in 3-month-old rats exposed to alcohol and nicotine, reported inflammatory infiltration of the stromal tissue, reduced acinar number and secretion, flattening of the mucosal folds, decreased nuclear volume, and stromal hypertrophy. Columnar epithelial atrophy and prostatic intraepithelial neoplasia were also observed.

In adult mice chronically consuming alcohol, the prostate exhibited a reduction in acinar number and mucosal folds, pronounced atrophy of the secretory epithelium, and significant stromal collagen deposition [76].

Martinez F.E. et al. [119] demonstrated that prolonged exposure of rats to 35% ethanol induced ultrastructural alterations in the ventral prostate epithelium, including dilated endoplasmic reticulum cisterns, reduced microvilli density, and irregular nuclear morphology. Ultrastructural examination of the lateral and dorsal prostate lobes in rats subjected to chronic sugarcane brandy consumption revealed progressive degeneration of glandular epithelial cells [75, 94]. Sattolo S. et al. [153] confirmed these characteristic morphological changes in the ventral prostate of alcohol-fed rats. In mice chronically exposed to alcohol, Gomes I.C. et al. [96] observed decreased cell volume and alterations in the secretory organelles of the seminal vesicles.

CHAPTER II. DESIGN AND METHODOLOGY OF CONDUCTING A MACROSCOPIC RESEARCH

2.1-§. Analysis of the experimental research

The morphological study included 213 male white outbred rats, ranging in age from the neonatal period up to 18 months. To investigate age-related morphological changes in the rat prostate, animals from all stages of early and late postnatal ontogenesis were examined. The grouping of the experimental material is presented in Table 2.1.1.

The lactation-age periods were selected according to the laboratory animal age classification proposed by V.I. Zapadnyuk (1971), based on their physical development: on day 6, hair begins to appear and the ears open; on day 11, the incisors erupt; by day 16, the animals are fully covered with hair and their eyes open; by day 22, they begin leaving the nest.

For late postnatal ontogenesis, the age gradation of laboratory rats proposed by V.G. Makarov and M.N. Makarova (2013) was applied:

- 1 month infantile or immature stage;
- 3 months juvenile stage;
- 6–9 months young adults;
- 12 months mature or adult stage;

- 18 months old age.
- Laboratory animals were maintained under standard recommended conditions
 (Zapadnyuk I.P., Zapadnyuk V.I., Zacharia E.A., 1983) in specialized cages
 placed on shelves. Each cage was labeled with the animals' date of birth, the
 start date of the experiment, and the age of the experimental group.
- Vivarium rooms were cleaned daily in the morning. Animals that died during the experiment were buried in the ground after treatment with a 20% bleach solution.

Table 2.1.1

Distribution of rats by age and experimental period

group	name of	age	age of animals										
stomach	groups	earl	early postnatal				late						
nyh		ontogenesis				postnatal				general			
						ontogenesis				number			
													of
		newborns	6 days	11 days	16 days	21st day	1 month	3 months	6 months	9 months	12 months	18 months	animals
1	control	18	20	18	17	16	14	12	14	12	10	10	161
2	experimental steel	-	-	-	-	-	-	12	12	8	10	10	52
Total		18	20	18	17	16	14	24	26	20	20	20	213

All stages of the study were conducted in accordance with the "European Convention for the Protection of Vertebrate Animals used for Experimental and other Scientific Purposes" [Directive 2010/63/EU].

The experimental cohorts were organized concurrently, ensuring homogeneity of the laboratory animals with respect to age, body mass, housing conditions, and nutritional regimen. A total of sixteen groups were delineated: neonates (n = 18), 6-day-old subjects (n = 20), 11-day-old subjects (n = 18), 16-day-old subjects (n = 17), 21-day-old subjects (n = 16), 1-month-old subjects (n = 14), 3-month-old controls (n = 12), 6-month-old controls (n = 14), 9-month-old controls (n = 12), 12-month-old controls (n = 10), 18-month-old controls (n = 10), 3-month-old experimental group (n = 12), 6-month-old experimental group (n = 12), 9-month-old experimental group (n = 10), and 18-month-old experimental group (n = 10).

All animals had ad libitum access to food, primarily grains and vegetables.

In the experimental cohorts, a model of chronic alcoholism was established through compulsory ethanol administration. A 40% ethyl alcohol solution was delivered intragastrically via a metallic gavage tube at a dosage of 7 g/kg of body mass once per day for a month preceding the main observation period (Sidorov P.I., 2002). Furthermore, artificial polydipsia was induced by substituting the drinking water with a 5% ethanol solution sweetened with sucrose at a concentration of 5 g per 100 ml (Knyshova L.P., 2016). Animals in the control groups were administered equivalent volumes of 0.9% sodium chloride solution intragastrically

Rats were humanely euthanized by swift decapitation under ether anesthesia in accordance with established protocols (Sidorov P.I., 2002; Rybakova A.V., 2015; Koptyaeva K.E., 2018). Termination was performed on days 6, 11, 16, and 21 of life, as well as at the completion of 1, 3, 6, 9, 12, and 18 months, with all procedures carried out in the morning following an overnight fast. Throughout euthanasia and subsequent dissection, strict adherence to biosafety regulations and ethical standards for laboratory animal handling was maintained.

Prior to sacrifice, each animal's body mass was measured. Following laparotomy, the prostate gland was excised, and its external morphology was assessed. The organ's mass,

length, width, and thickness were determined. Body and prostate weights were measured using JW-1 precision electronic balances (e = 0.02 g; Acom Inc., South Korea), while linear dimensions were obtained using a calibrated ruler or millimeter-scale tape. The organ mass coefficient (MC) was calculated using the formula:

 $MC = Organ \ weight \ (g) \times 100\% MC = \frac{\text{\ lext}Organ \ \ weight}{\text{\ (g)}} \times 100\% MC = Body \ weight \ (g) \times 100\% MC = Bod$

Macroscopic anatomical dissection served as the primary method for assessing the biometric characteristics of the prostate. Morphometric analyses were conducted in compliance with the decision of the Ethics Committee of the Ministry of Health of the Republic of Uzbekistan, No. 4/17-1442, dated September 21, 2020.

For the human study component, ultrasonographic and anthropometric examinations of the prostate gland were performed on 1,544 males ranging from the neonatal period to advanced age. This included ultrasound evaluation and morphometric assessment of 154 mature (I–II age periods) and elderly individuals diagnosed with chronic alcoholism. The obtained data facilitated comprehensive statistical analysis, ensuring the reliability and validity of the results.

The scheme of age periodization of human ontogenesis developed by Institute of Physiology of Children and Adolescents:

```
- newborns -0-10 days;
```

- \inf \inf
- early childhood -1–3 years;
- first childhood -4-7 years;
- second childhood -8-12 years old boys;
- adolescence 13–16 years old boys;
- adolescence 17–21 years old boys;
- first mature age -22-35 years of age for men;
- the second mature age -36-60 years of age for men;
- old age -61–74 years old men;
- old age -75–90 years;

Ultrasonographic evaluations and anthropometric assessments of somatic

development in neonatal males were carried out in the maternity unit of the Bukhara Regional Perinatal Center. Male subjects under the age of 16 years were examined using a MINDRAY DCN6 ultrasound diagnostic system (XXR, 2019) at the Nasriddin-Shams Multidisciplinary Private Clinic, Bukhara. Adult participants aged over 16 years underwent imaging at the Bukhara Multidisciplinary Regional Hospital and the Regional Narcological Dispensary, employing a SONOACE R3 ultrasound apparatus (South Korea, 2016).

2.2-§. Characteristics of the Applied Research Methods

During sonographic assessment, the transverse (width), anteroposterior (thickness), and longitudinal (length) dimensions of the prostate gland were recorded. The organ's volume was then calculated according to the formula described by Mitterberger et al. (Michael Mitterberger, Wolfgang Horninger, Friedrich Aigner, Germar M. Pinggera, Ilona Steppan, Peter Rehder, and Ferdinand Frauscher, 2019), which demonstrates the highest correlation with actual prostate volume measurements. The formula applied was:

 $V=T\times W\times D\times \pi 6V=T$ \times W \times D \times \frac{\pi}{6}V=T\times W\times D\times 6\pi where TTT represents the thickness, WWW the width, DDD the length of the prostate gland, and π \pi π is approximated as 3.14.

"Anthropometric evaluations of pediatric participants were carried out in the clinical rooms of the respective healthcare institutions under the supervision of a physician and assisted by a nurse. Prior to inclusion in the study, written informed consent was obtained from the parents or legal guardians of all children and adolescents. The assessment of physical development parameters followed the methodological guidelines described in *Morphometric Characteristics for Assessing the Physical Development of Children and Adolescents* (Tashkent, 1998) authored by Kh.N. Shamirzaev, S.A. Ten, and Sh.I. Tukhtanazarova.

Body length (stature) was determined using a calibrated stadiometer. Each subject stood barefoot on the base platform with the heels, buttocks, interscapular region, and occiput in contact with the vertical board of the instrument. The arms were positioned naturally along the sides of the body, heels together, and toes

directed slightly outward. The head was oriented so that the infraorbital margin and the superior margin of the auricular tragus lay in a horizontal plane (Frankfurt horizontal). The movable headpiece of the stadiometer was then lowered until it touched the crown of the head, compressing the hair to ensure accuracy.

For participants younger than two years, body length was assessed using a specially adapted infant stadiometer, consisting of a wooden measuring board 80 cm in length and 40 cm in width, equipped with a fixed headpiece at the upper end. Centimeter graduations were marked along the left edge, and a movable footboard was used to determine length. The child was positioned supine on the board, with the occiput resting firmly against the fixed headpiece. The head was gently stabilized, knees extended without force, and the movable footboard was adjusted to contact the plantar surfaces to ensure precise measurement.

Body mass was determined using calibrated standard scales in the morning hours, on an empty stomach, following evacuation of the bowel and bladder, and with outer garments and footwear removed. For neonates and children up to one year of age, specialized pediatric medical balances were employed.

Thoracic circumference was measured at rest using a flexible standard measuring tape. The subject stood upright with heels together, knees extended, and arms initially raised. The tape was placed posteriorly beneath the inferior angles of the scapulae and anteriorly along the lower margin of the nipples, corresponding to the level of the fourth rib. During the reading, the tape was applied without undue compression of soft tissues, and the arms were lowered to the sides.

Statistical processing of the obtained data was performed using Microsoft Excel version 7.0 and Statistica software package version 6.0. The mean values (M), relative measures (P), and their standard errors (m) were determined. Comparative analysis was carried out employing Student's t-test, with differences regarded as statistically significant at a threshold of $P \le 0.05$.

To assess the association between sonographically determined biometric parameters of the prostate gland and indicators of physical development, the Pearson

product—moment correlation coefficient (*r*) was computed using the method of paired (double) correlation, as described by Mamatkulov B.M. (2013).

CHAPTER III. MACROSCOPIC STRUCTURE OF THE PROSTATE OF RATS OF THE CONTROL GROUP IN POSTNATAL ONTOGENESIS

3.1-§. Macroanatomy of the prostate gland of white rats in early postnatal ontogenesis

It was observed that in newborn rats, the prostate is situated in the pelvic cavity above the superior margin of the pubic symphysis. It lies in contact with the urinary bladder dorsally and envelops the urethra anteriorly. The gland exhibits a light pink color and a soft consistency. Throughout postnatal ontogenesis, both the color and consistency of the prostate remain unchanged. At birth, the rat prostate consistently displays a longitudinal-oval shape (Fig. 3.1.1).

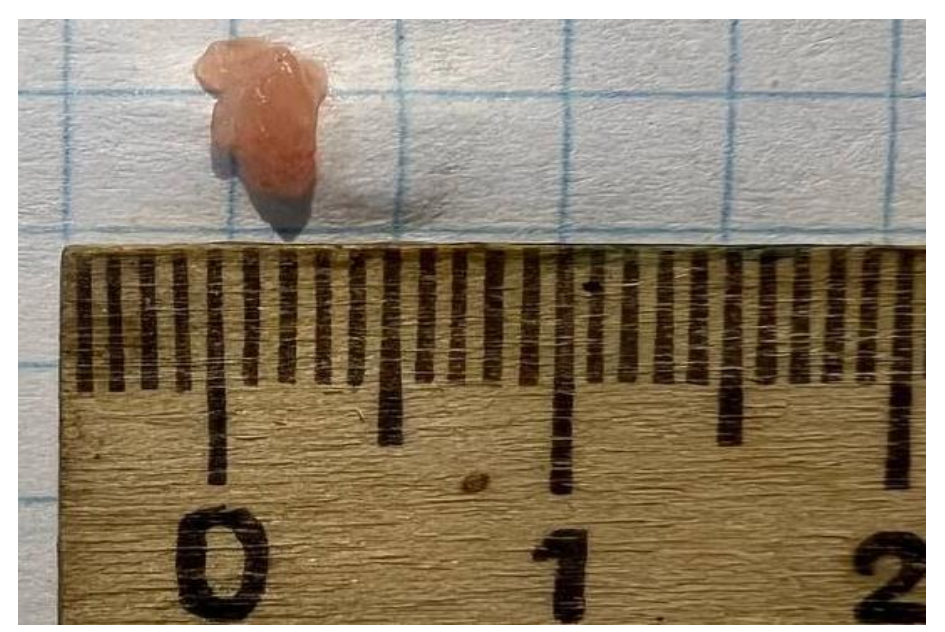


Fig.3.1.1.Prostate gland of longitudinal oval shape of newborn white rat. Magnified 4 times.

The study showed that the body weight of newborn animals is within the range of 4.4 - 5.92 grams, with an average of 5.16±0.1 grams (Fig. 3.1.2).



Fig.3.1.2. Newborn white rat weighing 5.92 grams. Increased by 2 times.

In neonatal rats, the prostate gland mass varies between 0.05 and 0.10 g, with a mean value of 0.08 ± 0.003 g. The organ mass coefficient is 1.55%. The anteroposterior dimension ranges from 1 to 2 mm, averaging 1.5 ± 0.07 mm; the transverse dimension spans 2–3 mm, with a mean of 2.2 ± 0.07 mm; and the longitudinal dimension extends from 3 to 4 mm, averaging 3.7 ± 0.07 mm.

From a topographical perspective, during the lactation period (up to 21 days of age), the prostate maintains both its anatomical position and characteristic light-pink coloration. In 6-day-old pups, the gland consistently presents a longitudinal-oval configuration (Fig. 3.1.3). At this developmental stage, body mass ranges from 10.0 to 11.9 g, averaging 10.92 ± 0.12 g, which corresponds to a 1.1-fold increase compared with the neonatal stage. The mean daily increment in body weight is 16.67%

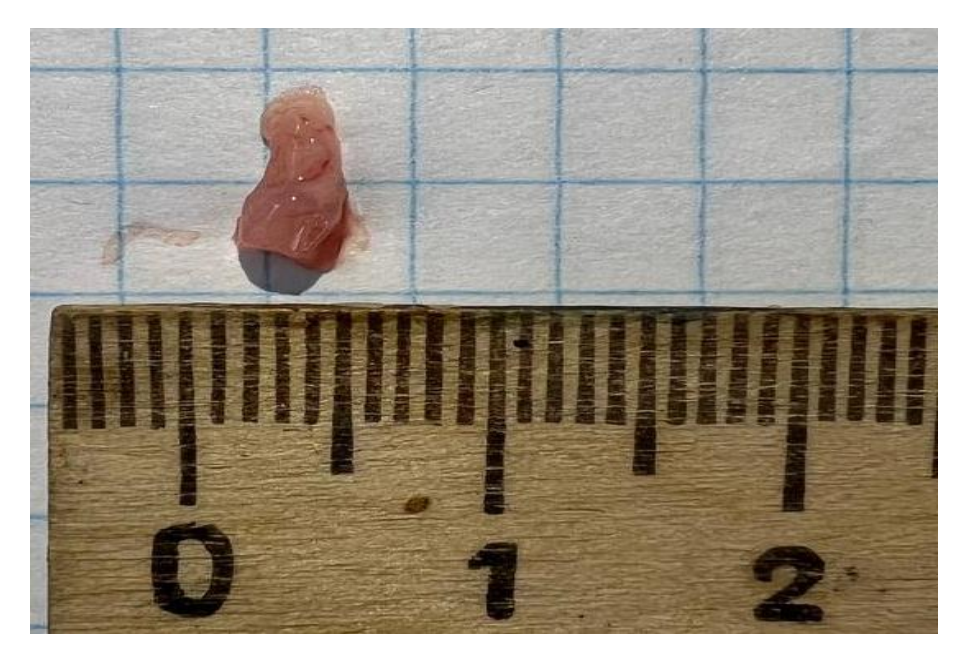


Fig.3.1.3.Prostate gland of longitudinal oval shape of 6-day old white rat. Enlarged by 4 times.

In 11-day-old rat pups, prostate gland mass ranges from 0.08 to 0.12 g, with a mean value of 0.10 ± 0.002 g, corresponding to a growth rate of 25.0%. The organ mass coefficient is 0.92%. The anteroposterior dimension varies between 1 and 2 mm, averaging 1.9 ± 0.06 mm, indicating a 26.7% increase. The transverse dimension spans 2–3 mm, with a mean of 2.5 ± 0.06 mm, representing a 15.2% increase, while the longitudinal measurement ranges from 4 to 5 mm, averaging 4.6 \pm 0.06 mm, reflecting a 22.6% increase.

Morphologically, on day 11, the gland most often retains a longitudinal-oval configuration (72.2%), whereas a rounded form is observed less frequently (27.8%) (Fig. 3.1.4). At this stage, body weight varies between 13.6 and 16.8 g, with a mean of 14.54 ± 0.21 g, corresponding to a 33.15% overall increase and an average daily gain of 20.0%.

In another subset of 11-day-old rats, prostate gland mass ranges from 0.09 to 0.15 g, averaging 0.13 ± 0.004 g, which signifies a 30.0% increase compared with the preceding age group. The organ mass coefficient at this developmental period is 0.89%.

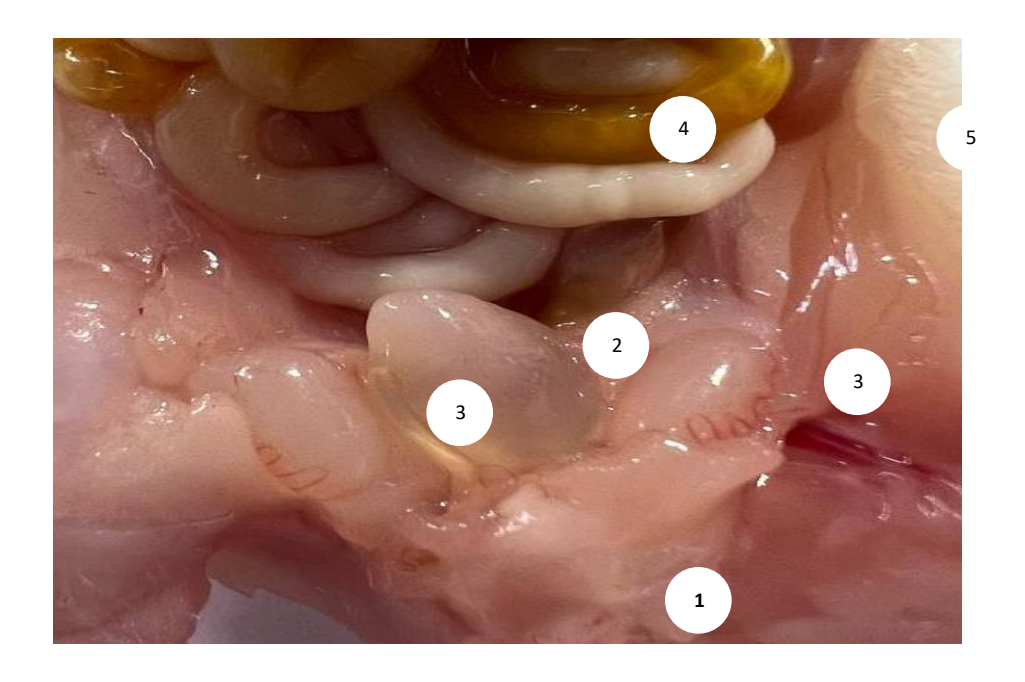


Fig.3.1.4.Topography of the prostate of an 11-day-old white rat. Magnified 6 times.

1-round prostate, 2-bladder, 3-testicles,

4-intestinal loops, 5-spleen.

In 16-day-old rats, the anteroposterior dimension of the prostate gland ranges from 2 to 3 mm, with an average of 2.3 ± 0.07 mm, representing a 21.1% increase relative to the preceding developmental stage. The transverse measurement varies between 2 and 4 mm, averaging 3.1 ± 0.13 mm, corresponding to a 24.0% growth, while the longitudinal dimension spans 4–6 mm, with a mean value of 5.3 ± 0.13 mm, indicating a 17.8% increase.

From a morphological perspective, the gland in 16-day-old pups predominantly retains a longitudinal-oval configuration (76.5%), whereas a rounded shape is observed in 23.5% of cases. At this age, body mass ranges from 14.6 to 18.4 g, averaging 16.24 ± 0.27 g, reflecting an 11.69% increase and a mean daily weight gain of 20.0% (Fig. 3.1.5).

The prostate mass during this stage ranges from 0.11 to 0.17 g, with a mean of 0.15 ± 0.004 g (Fig. 3.1.6), which corresponds to a 15.4% increase over the previous age group. The organ mass coefficient is calculated at 0.92%.



Fig.3.1.5.16-day-old white rat weighing 17.40 grams. Increased by 2 times.



Fig.3.1.6.Prostate gland of longitudinal oval shape of a 16-day old white rat weighing 0.11 grams. Increased by 2 times.

In 21-day-old rats, the anteroposterior dimension of the prostate gland varies from 2 to 4 mm, with a mean value of 2.8 ± 0.14 mm, representing a 21.7% increase compared with the preceding stage. The transverse measurement ranges between 3

and 4 mm, averaging 3.5 ± 0.07 mm, corresponding to a 12.9% growth, while the longitudinal length fluctuates from 5 to 7 mm, with an average of 6.3 ± 0.14 mm, indicating an 18.9% increase.

By the conclusion of the lactation period (day 21), the prostate maintains a longitudinal-oval configuration in 87.5% of examined specimens, whereas a rounded morphology is observed in 12.5% of cases (Fig. 3.1.7; Table 3.1.1). At this developmental stage, body mass ranges from 27.8 to 34.2 g, with a mean of 30.4 ± 0.47 g, reflecting an overall gain of 87.2% and an average daily weight increase of 20%



Fig.3.1.7. Round prostate gland of a 21-day-old white rat. Enlarged by 2 times.

At one month of age, the prostate gland in rats exhibits a mass ranging from 0.16 to 0.22 g, with a mean value of 0.19 ± 0.004 g. Body mass shows a 26.7% increase, and the organ mass coefficient is calculated at 0.63%.

The anteroposterior dimension of the gland spans 3–5 mm, averaging 3.6 ± 0.15 mm, representing a 28.6% increase. The transverse width varies between 4 and 6 mm, with a mean of 4.6 ± 0.15 mm, reflecting a 31.4% growth, while the longitudinal length ranges from 7 to 9 mm, averaging 7.9 ± 0.15 mm, corresponding to a 25.4% increase (Fig. 3.1.2).

Table 3.1.1

Percentage of prostate gland forms during postnatal ontogenesis

form	longitudinal-	rounded	two-lobed	quadripartite
	oval			
age				
newborn	100%	-	-	-
daily				
6-day	100%			
11-day	72.2%	27.8%	-	-
16 1	76.50/	22.50/		
16 days	76.5%	23.5%	-	-
21 days	87.5%	12.5%	_	-
1 month old	78.6%	21.4%	-	-
3 months	83.3%	16.7%	-	-
6 months	_		78.6%	21.4%
			70.070	21.176
9 months	-	-	16.7%	83.3%
12 months	-	-	-	100%
18 months	-	-	-	100%

Table 3.1.2

Organometric indices of the prostate of control group rats in early postnatal ontogenesis

parameters	body weight	average daily	prostate	organ mass	thickness	width	length
	of rats	growth (%)	weight	coefficient	(mm)	(mm)	(mm)
age	(gram)		(gram)	(%)			
newborns	4.4-5.9		0.05-0.10	0.89-2.17	1-2	2-3	3-4
	5.16±0.10			1.55±0.09			
			0.08 ± 0.003		1.5±0.07	2.2±0.07	3.7±0.07
6-day	10.0-11.9	16.67	0.08-0.12	0.67-1.11	1-2	2-3	4-5
	10.92±0.12*			0.92±0.03*			
			0.10±0.002*		1.9±0.06*	2.5±0.06	4.5±0.06*
11-day	13.6-16.8	20.0	0.09-0.15	0.65-1.10	2-3	2-4	4-6
	14.54±0.21*			0.89 ± 0.04			
			0.13±0.004*		2.3±0.07*	3.1±0.13*	5.3±0.13*
16 days	14.60-18.4	20.0	0.11-0.17	0.64-1.16	2-4	3-4	5-7

	16.24±0.27*			0.92±0.04			
			0.15±0.004		2.8±0.14	3.5±0.07	6.3±0.14*
21 days	27.80-34.2	20.0	0.16-0.22	0.50-0.77	3-5	4-6	7-9
	30.40±0.47*			0.63±0.02*			
			0.19±0.004*		3.6±0.15	4.6±0.15*	7.9±0.15*

Note: * - significance of differences in relation to the previous age (P \leq 0.05).

3.2 -§. Macroanatomical characteristics of the rat prostate in late postnatal ontogenesis

In 1-month-old (infantile) rats, the prostate gland is situated in the pelvic cavity beneath the urinary bladder, in contact posteriorly with the anterior surface of the pubic symphysis, and with the rectum located behind it (Fig. 3.2.1). At this age, the gland predominantly exhibits a longitudinal-oval shape in 78.6% of cases, while 21.4% display a rounded form.

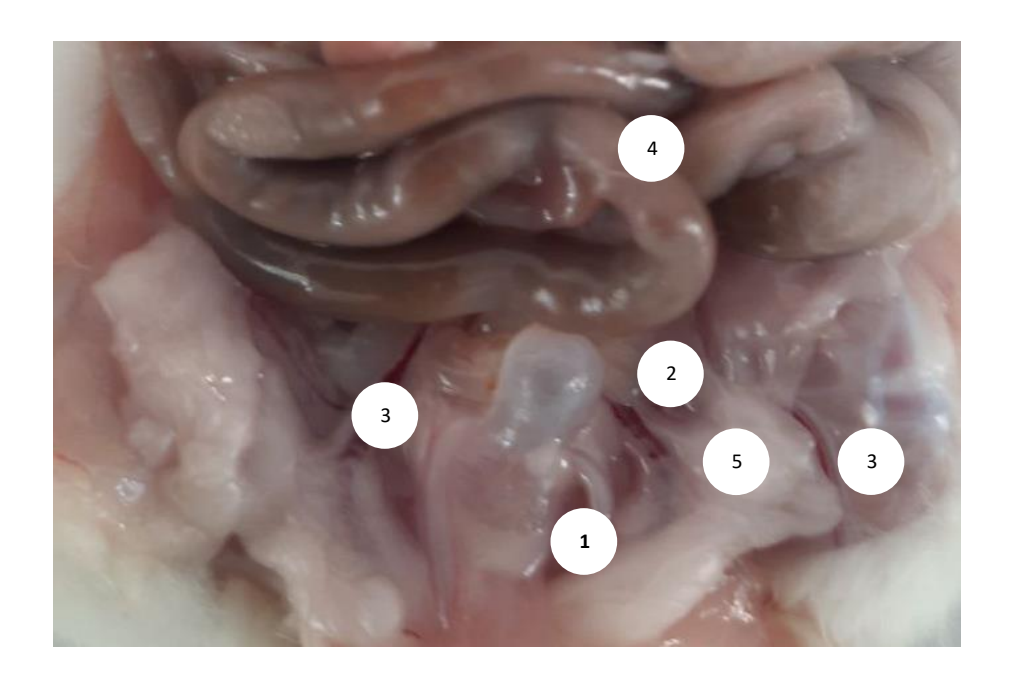


Fig.3.2.1. Topography of the prostate of a 1-month-old rat. Magnified by 2 times. 1-round prostate, 2-urinary bladder, 3-testicles, 4-intestinal loops, 5-vas deferens.

In infantile rats, body weight ranges from 38.6 to 48.0 grams, with an average of 42.78 ± 0.77 grams. The body weight growth rate is 40.72%, and the average daily increase is 11.15%. The prostate gland weighs between 0.17 and 0.28 grams, averaging 0.24 ± 0.009 grams, with a growth rate of 26.3% and a mass coefficient of 0.56%.

The anteroposterior dimension of the prostate gland ranges from 4 to 5 mm, with a mean of 4.3 ± 0.08 mm, corresponding to a 19.4% increase in thickness. The transverse measurement spans 4–7 mm, averaging 5.3 ± 0.25 mm, reflecting a 15.2% increase in width. The longitudinal length varies between 8 and 10 mm, with a mean of 9.0 ± 0.16 mm, indicating a 13.9% increase in length.

In juvenile rats (3 months old), the prostate remains located within the pelvic cavity beneath the urinary bladder, posteriorly adjacent to the anterior surface of the pubic symphysis, and anterior to the rectum (Fig. 3.2.2). Morphologically, the gland predominantly presents a longitudinal-oval configuration in 83.3% of specimens, while a rounded shape is observed in 16.7% of cases. At this developmental stage, body mass ranges from 104.1 to 117.1 g, averaging 110.68 ± 1.2 g, which represents a 1.6-fold increase relative to the previous age group, with an average daily weight gain of 1.66%.

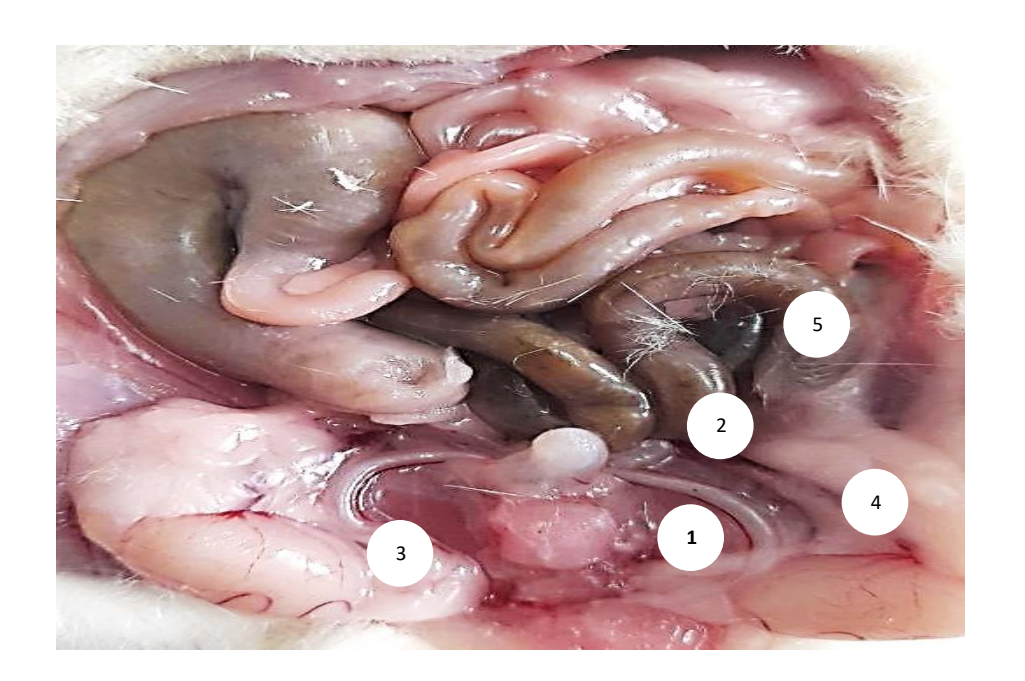


Fig.3.2.2.Topography of the prostate of a 3-month-old rat from the control group. Magnified 4 times. 1-round prostate gland, 2-urinary bladder, 3-testicles, 4-vas deferens, 5-loop of the colon.

The prostate gland in juvenile rats weighs between 0.26 and 0.39 grams, with an average of 0.34 ± 0.001 grams (Fig. 3.2.3). The organ's weight shows a 41.7% increase, and the mass coefficient of the prostate is 0.21%.



Fig.3.2.3. Longitudinal-oval prostate gland of a 3-month-old white rat from the control group weighing 0.29 grams. Increased by 2 times.

The anteroposterior dimension of the prostate gland in six-month-old rats ranges from 4 to 6 mm, averaging 5.0 ± 0.18 mm, reflecting a 16.3% increase in thickness. The transverse measurement varies between 5 and 7 mm, with a mean of 6.2 ± 0.18 mm, corresponding to a 17.0% increase in width. The longitudinal length spans 8–11 mm, averaging 10.1 ± 0.28 mm, indicating a 12.1% increase in length.

At this age, the prostate typically presents either a bilobed or quadrilobed morphology. In the bilobed configuration (78.6% of cases), both lobes are oblong-oval and oriented longitudinally. The gland is situated beneath the urinary bladder, enveloping the proximal portion of the vas deferens and extending along the lateral wall of the urethra. The overall size of the prostate exceeds that of the empty bladder.

In the quadrilobed form (21.4%), the organ comprises four paired lobes, distinguished according to their position relative to the bladder: ventral, dorsal, lateral, and anterior lobes. The ventral lobe is located immediately beneath the bladder, above the superior edge of the pubic bone, and accounts for approximately half of the total prostate mass. The dorsal lobe lies below and posterior to the attachment of the seminal vesicle and coagulating gland, surrounding the urethra dorsally. The lateral lobe is positioned beneath the seminal vesicle and coagulating gland. Due to their similar histological characteristics, the dorsal and lateral lobes

are often collectively designated as the dorsolateral lobe. The anterior lobes, or coagulating glands, are longitudinally elongated, convoluted tubular structures aligned along the lesser curvature of the seminal vesicles.

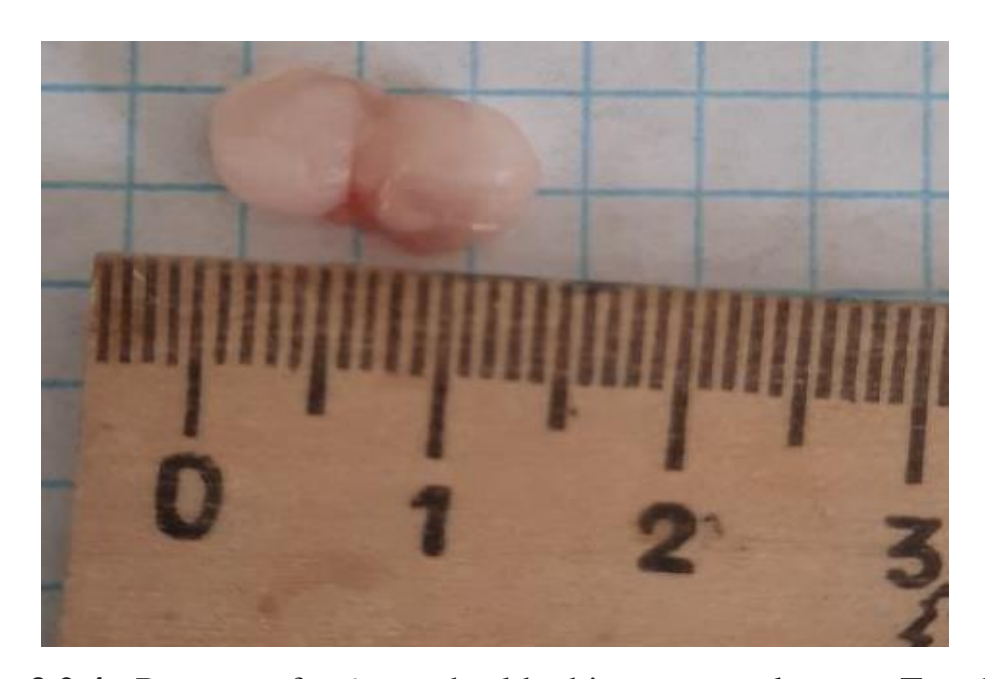


Fig.3.2.4. Prostate of a 6-month-old white ratcontrol group. Two-lobed structure. Increased by 2 times.

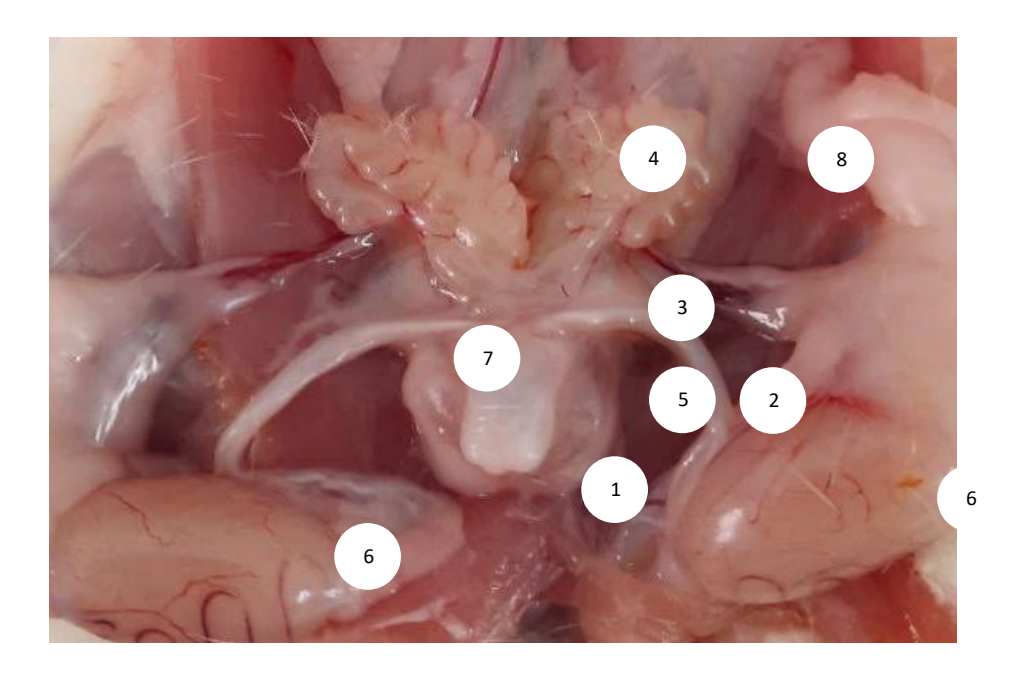


Fig.3.2.5. Topography of the prostate6-timonth-old rats of the control group. Four-lobed structure. Increased by 4 times. 1-ventral lobes of the prostate, 2-lateral lobes of the prostate, 3-dorsal lobes of the prostate, 4-anterior prostate

(coagulating gland), 5-urinary bladder, 6-testicles, 7-vas deferens, 8-seminal vesicles.

At six months of age, rats display body masses ranging from 204.4 to 225.4 g, with a mean of 213.07 ± 1.72 g. The overall body weight gain at this stage is 92.5%, with an average daily increment of 1.1%.

The prostate gland in six-month-old rats weighs between 0.31 and 0.83 g, averaging 0.60 ± 0.04 g. The organ exhibits a growth rate of 76.5%, and the mass coefficient is 0.28%.

Morphometric assessment indicates that the anteroposterior dimension of the prostate ranges from 5 to 8 mm, with a mean of 6.7 ± 0.25 mm, representing a 34.0% increase in thickness. The transverse dimension varies between 7 and 10 mm, averaging 8.9 ± 0.25 mm, reflecting a 43.5% increase in width. The longitudinal length fluctuates from 10 to 15 mm, with a mean of 13.0 ± 0.41 mm, corresponding to a 28.7% increase in length.

By nine months of age, the prostate demonstrates pronounced structural differentiation, presenting a bilobed configuration in 16.7% of animals and a quadrilobed configuration in 83.3% of cases (Fig. 3.2.6). At this developmental stage, body mass ranges from 280.4 to 296.7 g, with an average of 289.01 ± 1.5 g. The cumulative body weight gain during this period is 35.64%, with an average daily increase of 1.1%."



Fig.3.2.6. Prostate of a 9-month-old white ratcontrol group. Four-lobed structure. Increased by 2 times. 1-ventral lobes of the prostate, 2-lateral lobes of the prostate, 3-dorsal lobes of the prostate.

In rats aged 12 to 18 months, the prostate gland exhibits a mass ranging from 0.66 to 1.09 g, with a mean value of 0.91 ± 0.04 g. This corresponds to a 51.7% increase in organ mass, and the mass coefficient is calculated at 0.31%.

Morphometric evaluation reveals that the anteroposterior dimension of the prostate spans 6–8 mm, averaging 7.5 ± 0.18 mm, reflecting an 11.9% increase in thickness. The transverse measurement varies from 12 to 18 mm, with a mean of 15.0 ± 0.55 mm, indicating a 68.55% increase in width. The longitudinal length ranges between 11 and 16 mm, averaging 14.1 ± 0.46 mm, representing an 8.5% increase compared with the previous stage.

At one to one-and-a-half years of age, the prostate consistently demonstrates a quadrilobed configuration (Table 3.1.1). The ventral lobe is composed of two oval-shaped lobes situated ventrolaterally relative to the urinary bladder. The dorsolateral prostate, formed by the lateral and dorsal lobes, lies posterior to the bladder and seminal vesicles, oriented parallel to the urethra, with its posterior surface adjacent to the descending colon. Both lobes are positioned above the superior margin of the

pubic symphysis. The anterior lobes, or coagulating glands, are elongated tubular structures aligned along the lesser curvature of the seminal vesicles.

By the 12th month of life, the rats' body weight ranges from 303.4 to 325.4 grams, averaging 315.37 ± 2.38 grams, with a body weight increase of 9.12% and an average daily gain of 1.1%.

At 12 months of age, the prostate gland in rats ranges in weight from 0.86 to 1.34 grams, with an average of 1.12 ± 0.05 grams. The organ shows a mass increase of 23.1%, with a mass coefficient of 0.36%.

"The anteroposterior dimension of the prostate gland ranges from 6 to 9 mm, with a mean value of 7.9 ± 0.32 mm, reflecting a 23.1% increase in thickness. The transverse measurement varies between 14 and 18 mm, averaging 16.1 ± 0.43 mm, corresponding to a 7.3% increase in width. The longitudinal length spans 13-17 mm, with a mean of 15.2 ± 0.43 mm, indicating a 7.8% increase in length.

By 18 months of age, corresponding to the senile stage, the body mass of rats ranges from 318.7 to 351.4 g, with a mean of 335.08 \pm 3.53 g. The overall body weight gain during this period is 6.25%, with an average daily increase of 0.56%.

In 18-month-old rats, the prostate gland exhibits a mass between 0.96 and 1.65 g, averaging 1.23 ± 0.07 g. The organ demonstrates a growth rate of 9.8% and a mass coefficient of 0.37% (Fig. 3.2.7)."



Fig.3.2.7. Prostate of a one and a half year old rat from the control group weighing 1.63 grams. Four-lobed structure. Increased by 2 times.

The anteroposterior size of the organ varies from 7 to 10 mm, on average - 8.4 \pm 0.32 mm. The rate of increase in the thickness of the gland is 9.8%. The transverse size of the prostate is within 16 - 20 mm, on average is 17.4 ± 0.43 mm. The rate of increase in the width of the organ is 8.1%. The longitudinal size of the prostate gland fluctuates within 14 - 18 mm, on average is 16.1 ± 0.43 mm. The rate of increase in the length of the organ is 5.9% (see Table 3.2.1).

Table 3.2.1

Organometric indices of the prostate of control group rats in late postnatal ontogenesis

parameters	body weight	average daily	prostate	organ mass	thickness	width	length
	of rats	growth (%)	weight	coefficient	(mm)	(mm)	(mm)
age	(gram)		(gram)	(%)			
1 month old	38.6-48.0	11.2	0.17-0.28	0.38-0.69	4-5	4-7	8-10
	42.78±0.8*		0.24±0.009*	0.56±0.03	4.3±0.08*	5.3±0.25	9.0±0.16*
3 months	104.1-117.1	1.66	0.26-0.39	0.13-0.35	4-6	5-7	8-11
	110.68±1.2*		0.34±0.01*	0.21±0.01*	5.0±0.18	6.2±0.18	10.1±0.28
6 months	204.4-225.4	1,1	0.31-0.83	0.15-0.38	5-8	7-10	10-15
	213.07±1.7*		0.60±0.04*	0.28±0.02	6.7±0.25*	8.9±0.25*	13.0±0.41*
9 months	280.4-296.7	1,1	0.66-1.09	0.23-0.38	6-8	12-18	11-16
	289.01±1.5*		0.91±0.04*	0.31±0.01	7.5±0.18	15.0±0.55*	14.1±0.46
12 months	303.4-325.4	1,1	0.86-0.34	0.27-0.42	6-9	14-18	13-17
	315.37±0.05*		1.12±0.05	0.36±0.02	7.9±0.32	16.1±0.43	15.2±0.43

18 months	318.7-351.4	0.56	0.96-1.65	0.28-0.48	7-10	16-20	14-18
10 111011111	335.08±3.5*		1.23±0.07	0.37 ± 0.02	8.4±.32	17.4±0.43	16.1±0.43

Note: * - significance of differences in relation to the previous age ($P \le 0.05$).

CHAPTER IV. ANATOMY OF THE PROSTATE GLAND OF RATS OF THE EXPERIMENTAL GROUP

4.1-§. Macroanatomy of the rat prostate under chronic alcohol exposure

In the experimental cohort of 3-month-old juvenile rats, the prostate was located on the anterior surface of the pubic symphysis, beneath the urinary bladder. Morphologically, the gland presented a longitudinal-oval configuration in 66.7% of the subjects, whereas a rounded shape was observed in 33.3% of the animals. (Fig. 4.1.1).

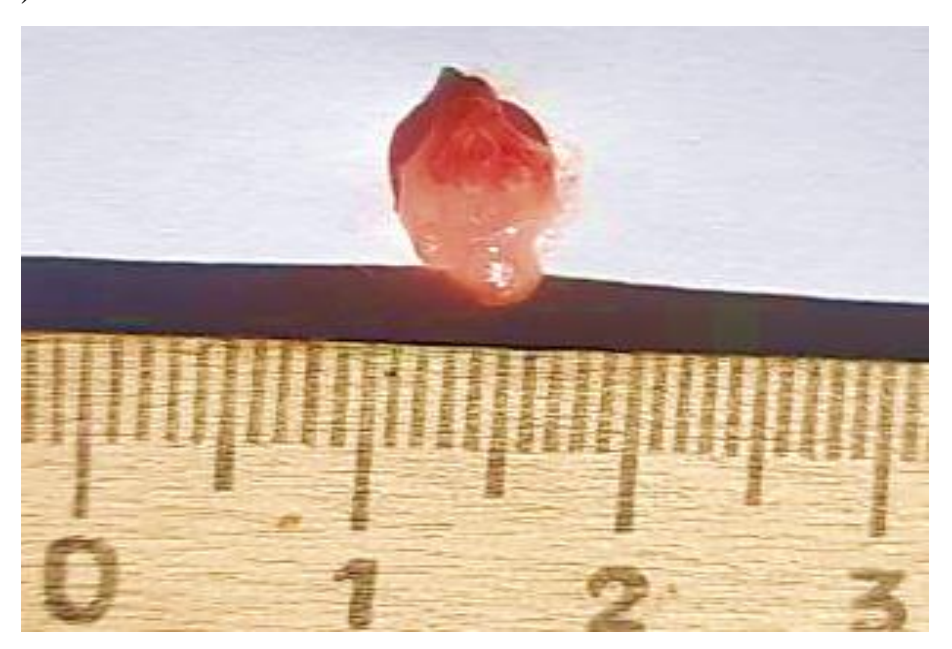


Fig.4.1.1. The prostate gland of an elongated oval shape of a 3-month-old white rat from the experimental group. Enlarged by 4 times.

In the experimental group of 3-month-old rats, body mass ranged from 65.2 to 83.4 g, with a mean of 75.6 ± 1.67 g, representing a 31.73% reduction compared with age-matched controls. The prostate gland mass varied between 0.10 and 0.28 g, averaging 0.20 ± 0.02 g, indicating a 41.2% decrease relative to control animals. The organ mass coefficient was 0.26%.

Morphometric assessment revealed that the anteroposterior dimension of the prostate measured 3–5 mm, with a mean of 4.0 ± 0.18 mm, which is 20.0% smaller than that of controls. The transverse width ranged from 4 to 6 mm, averaging 5.1 ± 0.18 mm, reflecting a 17.7% reduction compared with the control group. The longitudinal length varied between 6 and 9 mm, with a mean of 7.9 ± 0.28 mm, corresponding to a 21.8% decrease relative to age-matched controls.

At six months of age, the prostate in experimental rats displayed either a bilobed configuration (83.3%) or a quadrilobed configuration (16.6%). In the bilobed form, both lobes were oblong-oval, located beneath the urinary bladder, extending along the lateral walls of the urethra, and enveloping the proximal segment of the vas deferens. In animals with a quadrilobed prostate (Fig. 4.1.2), the central lobes were positioned ventrally along the urethra immediately below the bladder, forming two oval-shaped structures that covered the initial urethral segment. The lateral ventral lobes lay beneath the seminal vesicles and coagulating glands, partially overlapping the ventral lobes and merging dorsally with the dorsal lobes. The dorsal lobes were situated posterior to the bladder, beneath and behind the attachment points of the seminal vesicles and coagulating glands. The anterior lobes, or coagulating glands, were elongated tubular structures aligned along the lesser curvature of the seminal vesicles.

The body mass of the rats varied between 182.1 and 203.8 g, with a mean value of 192.5 ± 2.0 g, representing a 9.67% reduction relative to age-matched controls. The mean daily weight increment was 1.1%.

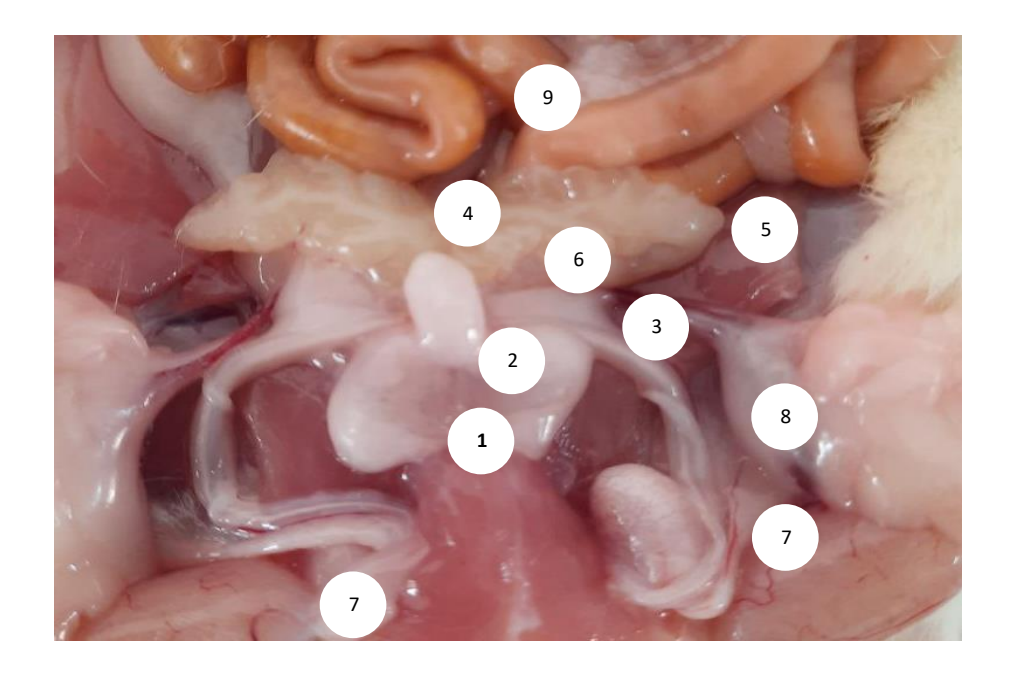


Fig.4.1.2. Prostate Topography in Six-Month-Old Experimental Rats: Four-lobed structure, magnified ×2. Key structures: 1 – ventral prostate lobes, 2 – lateral prostate lobes, 3 – dorsal prostate lobes, 4 – anterior prostate (coagulating gland), 5 – seminal vesicles, 6 – urinary bladder, 7 – testes, 8 – vas deferens, 9 – intestinal loops.

The prostate gland mass ranged from 0.18 to 0.63 g, with a mean of 0.45 \pm 0.04 g. Relative to age-matched controls, this represents a 25.0% reduction in mass, with a mass coefficient of 0.23%. The anteroposterior dimension of the gland measured 4–6 mm, averaging 5.7 \pm 0.18 mm, corresponding to a 14.9% decrease compared with controls. The transverse width varied between 7 and 11 mm, with a mean of 8.1 \pm 0.37 mm, reflecting a 9.0% reduction. The longitudinal length ranged from 7 to 13 mm, averaging 11.0 \pm 0.55 mm, indicating a 15.4% decrease relative to control animals.

In nine-month-old experimental rats, the prostate exhibited either a bilobed configuration (75.0%) or a quadrilobed configuration (25.0%)

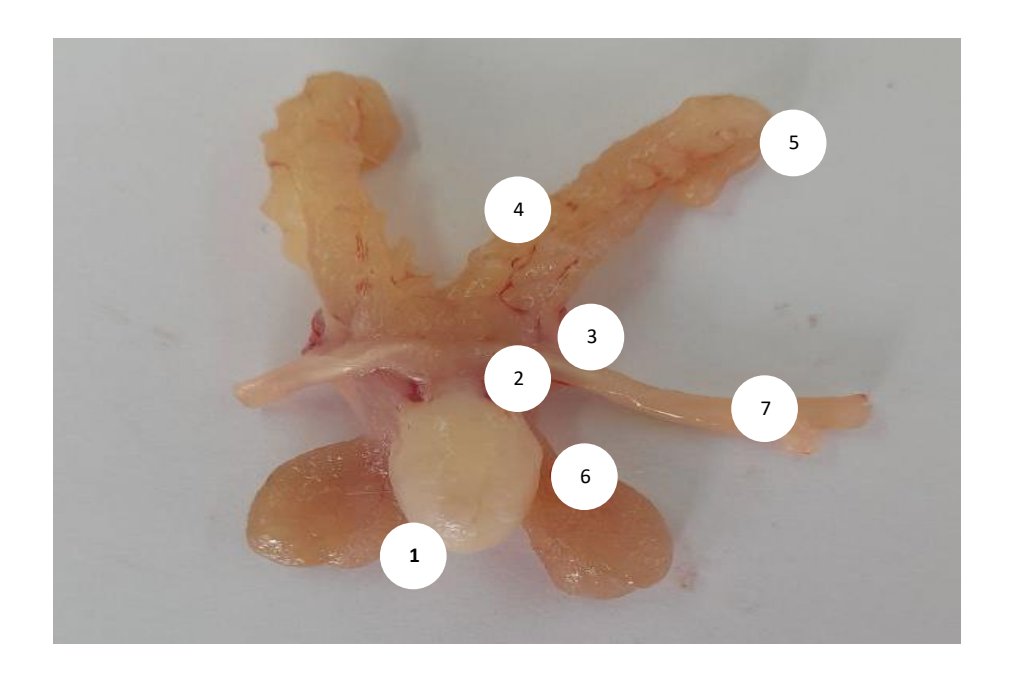


Fig.4.1.3.Prostate of a 9-month-old white rat from the experimental group. Four-lobed structure. Enlarged by 4 times. 1-ventral lobes of the prostate, 2-lateral lobes of the prostate, 3-dorsal lobes of the prostate, 4-anterior prostate (coagulating gland), 5-seminal vesicles, 6-urinary bladder, 7-vas deferens.

At nine months of age, the experimental rats exhibited body masses ranging from 235.6 to 256.1 g, with a mean of 245.2 ± 2.73 g. This corresponds to a 15.5% reduction relative to age-matched controls, with an average daily weight gain of 0.59%.

At this stage, the prostate gland mass varied between 0.61 and 1.04 g, averaging 0.85 ± 0.06 g. Compared with controls, the organ mass decreased by 6.6%, and the mass coefficient was 0.35%. Morphometric analysis revealed that the anteroposterior dimension of the gland ranged from 5 to 7 mm, averaging 6.5 ± 0.27 mm, reflecting a 13.3% reduction relative to controls. The transverse width spanned 11–17 mm, with a mean of 13.4 ± 0.8 mm, corresponding to a 10.6% decrease, while the longitudinal length ranged from 10 to 15 mm, averaging 12.2 ± 0.67 mm, indicating a 13.4% reduction compared with the control group.

By the twelfth month of the experiment, all rats displayed a quadrilobed prostate morphology. At this time, body mass ranged from 267.7 to 289.1 g, with an

average of 278.7 ± 2.31 g, representing an 11.63% reduction relative to controls, and an average daily weight gain of 1.1%.

In one-year-old rats from the experimental group, the prostate gland weight ranged from 0.80 to 1.27 grams, with a mean of 1.03 ± 0.05 grams (Fig. 4.1.4). Relative to the age-matched control group, this represents an 8.0% reduction in gland weight, and the mass coefficient was 0.37%.

The anteroposterior dimension of the prostate varied between 6 and 8 mm, averaging 7.0 ± 0.22 mm, which is 11.4% smaller than in controls. The transverse size ranged from 13 to 18 mm, with a mean of 15.2 ± 0.54 mm, showing a 5.6% decrease compared to the control group. The longitudinal length of the gland fluctuated between 11 and 16 mm, averaging 13.9 ± 0.54 mm, reflecting an 8.6% reduction relative to controls.



Fig.4.1.4. Prostate of a one-year-old white rat of the experimental group weighing 1.15 grams. Four-lobed structure. Enlarged by 2 times.

The study revealed that in 18-month-old rats of the experimental group, the prostate exhibited a two-lobed structure in 20% of cases (Fig. 4.1.5) and a four-lobed structure in 80% of cases (Table 4.1.1). Body weight ranged from 253.8 to 298.6 grams, with a mean of 267.0 ± 4.83 grams, representing a 20.32% decrease

compared to age-matched controls. The average daily weight gain decreased by 0.56%.

At this age, the prostate mass varied between 0.61 and 1.10 grams, averaging 0.80 ± 0.05 grams, reflecting a 35.0% reduction relative to the control group. The mass coefficient was 0.24%.

The anteroposterior dimension of the prostate ranged from 6 to 8 mm, with a mean of 7.1 ± 0.22 mm, a 15.5% reduction compared to controls. The transverse size varied from 12 to 17 mm, averaging 14.4 ± 0.54 mm, showing a 17.2% decrease. The longitudinal length of the gland fluctuated between 11 and 15 mm, with an average of 13.0 ± 0.43 mm, which is 19.3% smaller than in the control group (Table 4.1.2).

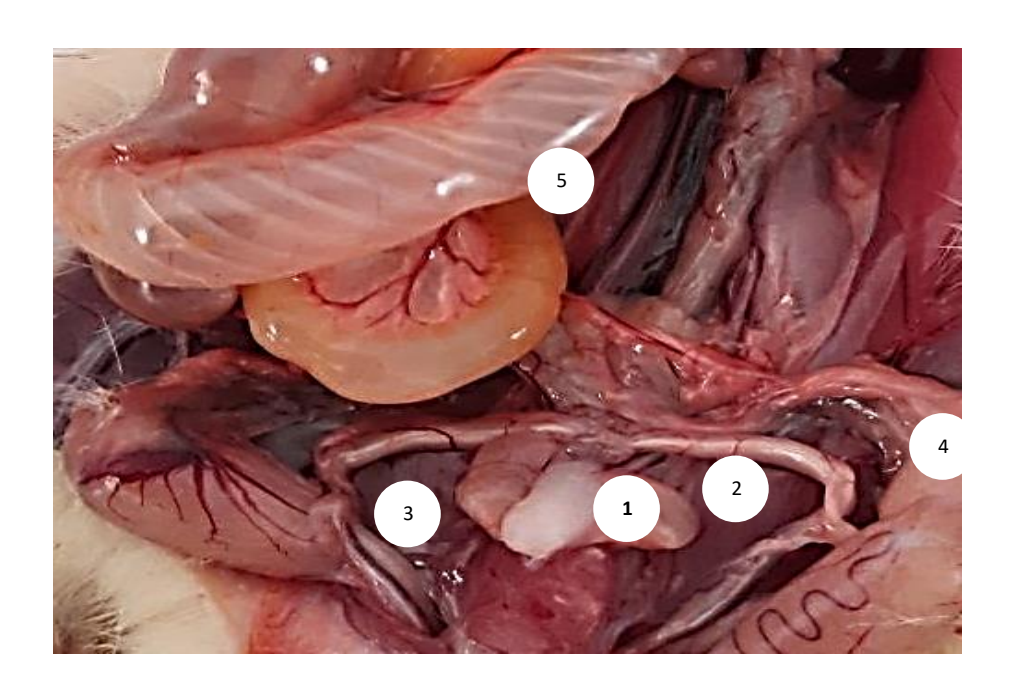


Fig.4.1.5.Topography of the prostate gland of an 18-month-old white rat from the experimental group. Magnified 4 times. 1-bilobed prostate, 2-urinary bladder, 3-testicles, 4-vas deferens, 5-intestinal loops.

Table 4.1.1

Percentage of prostate gland shapes in animals of the experimental group

form	longitudinal-	rounded	two-lobed	quadripartite
age	oval			
3 months	66.7%	33.3%	-	-
6 months	-	-	83.3%	16.7%
9 months	-	-	25.0%	75.0%
12 months	-	-	-	100%
18 months	-	-	20.0%	80.0%

Table 4.1.2.

Organometric indices of the prostate of rats of the experimental group

parameters	body weight	average daily	prostate	organ mass	thickness	width	length
	of rats	growth (%)	weight	coefficient	(mm)	(mm)	(mm)
age	(gram)		(gram)	(%)			
,	65.2-83.4		0.10-0.28	0.89-2.17	3-5	4-6	6-9
3 months	75.6±1.67*		0.20±0.02*	1.55±0.09	4.0±0.18	5.1±0.18*	7.9±0.28*
	182.1-203.8	1,1	0.18-0.63	0.67-1.11	4-6	7-11	7-13
6 months	192.5±2.0*		0.45±0.04	0.92±0.03*	5.7±0.18	8.1±0.37	11.0±0.55
	235.6-256.1	0.59	0.61-1.04	0.65-1.10	5-7	11-17	10-15
9 months	245.2±2.73*		0.85±0.06	0.89±0.04	6.5±0.27	13.4±0.80	12.2±0.67
	267.7-289.1	1,1	0.80-1.27	0.64-1.16	6-8	13-18	11-16
12 months	278.7±2.31*		1.03±0.05	0.92±0.04	7.0±0.22	15.2±0.54	13.9±0.54
	253.8-298.6	0.56	0.61-1.1	0.50-0.77	6-8	12-17	11-15
18 months	267.0±4.83*		0.80±0.05*	0.63±0.02*	7.1±0.22	14.4±0.54*	13.0±0.43*

Note: * - reliability of differences in relation to control($P \le 0.05$).

CHAPTER V. ULTRASONIC MORPHOMETRY OF ORGANOMETRIC PARAMETERS OF THE HUMAN PROSTATE DURING POSTNATAL ONTOGENESIS AND DURING CHRONIC ALCOHOL EXPOSURE

5.1-§. Age-Related Morphometry of Human Prostate Biometric Parameters Based on Ultrasonography

Ultrasonographic evaluation demonstrated that in neonates (1–10 days old), the anteroposterior dimension (thickness) of the prostate ranged from 5 to 11 mm, with a mean of 8.9 ± 0.32 mm. The transverse dimension (width) varied between 3 and 7 mm, averaging 4.8 ± 0.22 mm, whereas the longitudinal dimension (length/height) spanned 6–12 mm, with a mean of 9.8 ± 0.32 mm. The corresponding prostate volume at this stage fluctuated from 0.05 to 0.42 cm³, with an average of 0.24 ± 0.02 cm³.

During infancy (up to 1 year of age), the anteroposterior dimension of the gland was recorded between 6 and 12 mm, averaging 9.4 ± 0.25 mm, reflecting a growth rate of 5.6%. The transverse width ranged from 3 to 8 mm, with a mean of 5.15 ± 0.21 mm, corresponding to a 7.3% growth rate. The longitudinal dimension varied from 7 to 13 mm, averaging 10.36 ± 0.25 mm, indicating a growth rate of 5.7%. Prostate volume at this stage ranged between 0.07 and 0.66 cm³, with a mean of 0.29 ± 0.02 cm³, reflecting a 20.8% increase in volume.

In early childhood (1–3 years), the anteroposterior dimension of the prostate spanned 7–16 mm, with an average of 10.3 ± 0.27 mm, corresponding to a growth rate of 9.6%. The transverse dimension ranged from 4 to 10 mm, averaging 6.7 ± 0.18 mm, representing a significant growth rate of 30.1%. The longitudinal length varied between 8 and 16 mm, with a mean of 11.4 ± 0.21 mm, indicating a 10.0% increase compared with the previous stage.

.

Age-Related Morphometry of the Human Prostate Based on Ultrasonography (Early Childhood to Adolescence)

In early childhood (1–3 years), the prostate volume ranged from 0.12 to 1.1 cm³, with a mean of 0.45 ± 0.03 cm³, corresponding to a growth rate of 55.2%.

During the first stage of childhood (4–7 years), the anteroposterior (thickness) dimension of the prostate varied between 9 and 18 mm, averaging 12.5 ± 0.19 mm, reflecting a 21.4% increase. The transverse (width) dimension ranged from 5 to 12 mm, with a mean of 8.26 ± 0.15 mm, corresponding to a growth rate of 23.3%. The longitudinal (height) dimension spanned 9–20 mm, averaging 13.84 ± 0.23 mm, indicating a 21.4% increase relative to the previous stage. Prostate volume at this stage ranged from 0.25 to 1.8 cm³, with a mean of 0.77 ± 0.03 cm³, reflecting a growth rate of 71.7%.

In the second stage of childhood (8–12 years), the anteroposterior dimension of the gland varied between 10 and 23 mm, with a mean of 14.37 ± 0.26 mm, representing a growth rate of 15.0%. The transverse dimension ranged from 7 to 19 mm, averaging 11.1 ± 0.24 mm, corresponding to a 34.4% increase. The longitudinal dimension spanned 12–24 mm, with a mean of 16.27 ± 0.24 mm, reflecting a 17.6% growth. Prostate volume during this period fluctuated from 0.44 to 4.8 cm³, averaging 1.44 ± 0.09 cm³, indicating an 87.0% increase compared with the previous stage.

In adolescence (13–16 years), the anteroposterior dimension increased from 15 to 26 mm, averaging 19.9 ± 0.30 mm, corresponding to a 38.5% growth. The transverse width ranged from 14 to 33 mm, with a mean of 22.2 ± 0.51 mm, effectively doubling relative to the previous age period. The longitudinal dimension varied between 14 and 28 mm, averaging 20.6 ± 0.34 mm, reflecting a 26.6% increase. Prostate volume in adolescent boys ranged from 1.65 to 11.1 cm³, with a mean of 4.93 ± 0.25 cm³, representing a 3.4-fold increase compared with the prior stage.

Prostate Morphometry in Late Adolescence and Adulthood Based on Ultrasonography

In late adolescence (17–21 years), the anteroposterior (thickness) dimension of the prostate ranged from 21 to 32 mm, with a mean of 25.68 ± 0.20 mm, reflecting

a growth rate of 29.0%. The transverse (width) dimension varied between 26 and 39 mm, averaging 33.9 ± 0.23 mm, corresponding to a 52.7% increase. The longitudinal (length) dimension fluctuated from 20 to 30 mm, with a mean of 27.6 ± 0.18 mm, indicating a 34.0% growth. Prostate volume in young adult males ranged from 5.7 to 20.6 cm³, with a mean of 11.6 ± 0.27 cm³, representing a 2.4-fold increase compared to adolescence.

In the first period of mature adulthood (22–35 years), the anteroposterior dimension of the gland ranged from 24 to 32 mm, averaging 27.4 ± 0.14 mm, with a growth rate of 6.7%. The transverse width varied between 29 and 41 mm, with a mean of 35.8 ± 0.22 mm, reflecting a 5.6% increase. The longitudinal dimension spanned 24–35 mm, averaging 27.7 ± 0.20 mm, showing a minimal growth of 0.4%. Prostate volume in men of this age group ranged from 8.7 to 24.0 cm³, with a mean of 14.2 ± 0.28 cm³, corresponding to a 22.4% increase relative to late adolescence.

In the second period of mature adulthood (36–59 years), the thickness of the prostate varied from 26 to 36 mm, with a mean of 31.2 ± 0.18 mm, indicating a growth rate of 13.8%. The transverse width ranged between 34 and 46 mm, averaging 41.1 ± 0.22 mm, reflecting a 14.8% increase. The longitudinal dimension of the gland fluctuated from 26 to 35 mm, with a mean of 31.0 ± 0.16 mm, corresponding to an 11.9% growth in length.

Prostate Morphometry in Middle-Aged and Elderly Men Based on Ultrasonography

In the second period of middle adulthood (36–59 years), the prostate volume ranged from 12.0 to 30.3 cm³, with a mean of 20.8 ± 0.33 cm³, corresponding to a growth rate of 46.5%.

In elderly men aged 60–74 years, the anteroposterior (thickness) dimension of the prostate varied from 30 to 40 mm, with a mean of 34.5 ± 0.22 mm, reflecting a 10.6% increase. The transverse (width) dimension ranged from 38 to 49 mm, averaging 45.1 ± 0.24 mm, corresponding to a 9.7% growth. The longitudinal (length/height) dimension fluctuated between 30 and 41 mm, with a mean of 37.2 ± 0.24 mm, indicating a 20.0% increase. The prostate volume in this age group ranged

from 17.9 to 42.0 cm³, with a mean of 30.3 ± 0.53 cm³, representing a 45.7% increase.

In men of advanced age (75–90 years), the gland thickness ranged from 32 to 40 mm, with an average of 35.2 ± 0.36 mm, reflecting a growth rate of 2.0%. The transverse dimension varied between 44 and 50 mm, averaging 46.5 ± 0.27 mm, corresponding to a 3.1% increase. The longitudinal dimension fluctuated from 34 to 41 mm, with a mean of 38.2 ± 0.32 mm, indicating a 2.7% increase. The prostate volume ranged from 25.0 to 42.9 cm³, with a mean of 32.7 ± 0.81 cm³, showing a 7.9% growth (see Table 5.1.1).

Table 5.1.1.

Morphometric characteristics of ultrasound parameters of the prostate gland of males in postnatal ontogenesis

parameters	thickness	width	length	volume
age	(mm)	(mm)	(mm)	(cubic cm)
newborns	5-11	3-7	6-12	0.05-0.42
	8.9±0.32	4.8±0.22	9.8±0.32	0.24±0.02
infancy	6-12	3-8	7-13	0.07-0.66
	9.4±0.25	5.1±0.21	10.4±0.25	0.29±0.02
early	7-16	4-10	8-16	0.12-1.1
childhood	10.3±0.27	6.7±0.18*	11.4±0.21	0.45±0.03*
I - childhood	9-18	5-12	9-20	0.25-1.8
period	12.5±0.19*	8.3±0.15*	13.8±0.23*	0.77±0.03*
II - childhood	10-23	7-19	12-24	0.44-4.8
period	14.4±0.26*	11.1±0.24*	16.3±0.24*	1.44±0.09*
adolescence	15-26	14-33	14-28	1.65-11.1
	19.9±0.3*	22.2±0.51*	20.6±0.34*	4.93±0.25*

adolescence	21-32	26-39	20-30	5.7-20.6
	25.7±0.2*	33.9±0.23*	27.6±0.18*	11.6±0.27*
I – the period of	24-32	29-41	24-35	8.7-24.0
mature age	27.4±0.14*	35.8±0.22*	27.7±0.20	14.2±0.28*
II - the period of	26-36	34-46	26-35	12.0-30.3
mature age	31.2±0.18*	41.1±0.22*	31.0±0.16*	20.8±0.33*
old age	30-40	38-49	30-41	17.9-42.0
	34.5±0.22*	45.1±0.24*	37.2±0.24*	30.3±0.53*
old age	32-40	44-50	34-41	25.0-42.9
	35.2±0.36	46.5±0.27	38.2±0.32	32.7±0.81

Note: * - reliability of differences in relation to the previous age $(P \le 0.05)$.

5.2-§. Echographic characteristics of the prostate in men suffering from chronic alcoholism

Prostate Morphometry in Men with Chronic Alcoholism

The study demonstrated that in men of the first period of mature adulthood (22–35 years) with chronic alcoholism, the anteroposterior (thickness) dimension of the prostate ranged from 25 to 36 mm, averaging 31.2 ± 0.34 mm. Compared to agematched controls, this represents a 13.8% increase in thickness. The transverse (width) dimension varied from 33 to 43 mm, with a mean of 38.0 ± 0.31 mm, reflecting a 6.1% increase relative to controls. The longitudinal (height/length) dimension ranged from 31 to 43 mm, averaging 37.0 ± 0.37 mm, showing a 33.6% increase compared with the control group.

Prostate volume in this age group ranged from 13.8 to 34.8 cm³, with a mean of 22.95 ± 0.65 cm³, corresponding to a 61.3% increase relative to controls.

In men of the second period of mature adulthood (36–59 years) with chronic alcoholism, the anteroposterior dimension of the gland varied from 26 to 38 mm, averaging 32.4 ± 0.37 mm, which is a 3.8% increase compared with controls. The transverse dimension ranged from 36 to 48 mm, with a mean of 41.5 ± 0.37 mm, reflecting a 1.0% increase relative to age-matched controls. The longitudinal dimension fluctuated between 34 and 45 mm, averaging 39.9 ± 0.34 mm, representing a 28.7% increase in length compared to controls.

The volume of the prostate in the second period of middle age is in the range from 16.6 to 42.9 cm³, on average - 28.1±0.79 cm³. Compared with the control group, the volume of the gland increases by 35.1%.

Prostate Morphometry in Elderly Men with Chronic Alcoholism

The study demonstrated that in elderly men affected by chronic alcoholism, the anteroposterior (thickness) dimension of the prostate ranged from 33 to 46 mm, with a mean value of 40.5 ± 0.39 mm. Compared with age-matched controls, this corresponds to a 17.4% increase in thickness. The transverse (width) dimension varied between 44 and 56 mm, averaging 49.6 ± 0.36 mm, reflecting a 10.0% increase relative to the control group. The longitudinal (height/length) dimension ranged from 41 to 59 mm, with a mean of 47.3 ± 0.54 mm, representing a 27.2% increase compared to age-matched controls.

Prostate volume in this cohort ranged from 31.1 to 79.5 cm³, with a mean of 49.7 ± 1.45 cm³, indicating a 64.0% increase in volume relative to controls (see Table 5.2.1).

Table 5.2.1

Morphometric characteristics of ultrasound parameters of the prostate gland of men suffering from chronic alcoholism

parameters	thickness	width	length	volume
age	(mm)	(mm)	(mm)	(cubic cm)

I – the period of	25-36	33-43	31-43	13.8-34.8
mature age	31.2±0.34*	38.0±0.31*	37.0±0.37*	22.9±0.65*
II - the period of	26-38	36-48	34-45	16.6-42.9
mature age	32.4±0.37	41.5±0.37	39.9±0.34*	28.1±0.79*
old age	33-46	44-56	41-59	31.1-79.5
	40.5±0.39*	49.6±0.36*	47.3±0.54*	49.7±1.45*

Note: * - reliability of differences in relation to control $(P \le 0.05)$.

CHAPTER VI. ANTHROPOMETRIC CHARACTERISTICS OF HUMAN PHYSICAL DEVELOPMENT INDICATORS IN POSTNATAL ONTOGENESIS AND UNDER CHRONIC ALCOHOL EXPOSURE

6.1-§. Morphometric parameters of physical development of males in postnatal ontogenesis and its relationship with biometric indicators of the prostate

An anthropometric assessment revealed that the body height of newborn boys ranged from 46.1 to 53.2 cm, with a mean of 51.6 ± 0.43 cm. Body weight at this age was between 3.5 and 4.3 kg, averaging 4.0 ± 0.05 kg. Chest circumference at rest varied from 34.2 to 43.1 cm, with a mean of 37.8 ± 0.54 cm.

At the neonatal stage, the correlation coefficients (r) between prostate volume and anthropometric parameters were as follows: body height, 0.35; body weight, 0.22; chest circumference, 0.55.

During infancy, body height ranged from 68.4 to 75.3 cm, with a mean of 72.0 ± 0.39 cm, reflecting a growth rate of 39.5% relative to birth. Body weight increased 2.4-fold compared to the neonatal period, ranging from 8.4 to 11.1 kg, with a mean of 9.6 ± 0.15 kg. Chest circumference measured 47.1–51.4 cm, averaging 49.5 ± 0.25 cm, corresponding to a growth rate of 31.0%.

In infancy, the correlation coefficients between prostate volume and anthropometric indicators were: body height, 0.15; body weight, 0.17; chest circumference, 0.18.

In early childhood, boys exhibited a body height ranging from 79.6 to 92.6 cm, with an average of 87.8 ± 0.47 cm, indicating a growth rate of 21.9%. Body weight varied from 12.4 to 16.3 kg, averaging 14.3 ± 0.14 kg, reflecting a 49.0% increase. Chest circumference at rest ranged from 48.6 to 55.8 cm, with a mean of 51.7 ± 0.26 cm, corresponding to a growth rate of 4.4%.

At this stage of early childhood, the correlation coefficients (r) between prostate volume and anthropometric parameters were as follows: body height, 0.25; body weight, 0.10; chest circumference, 0.20.

During the first period of childhood (approximately 4–7 years), boys' body length ranged from 94.3 to 124.2 cm, with a mean of 109.8 ± 0.78 cm, representing a growth rate of 25.1%. Body weight varied between 13.4 and 31.3 kg, averaging 21.4 ± 0.47 kg, reflecting a 49.7% increase. Chest circumference at rest ranged from 50.3 to 61.8 cm, with a mean of 56.4 ± 0.30 cm, corresponding to a growth rate of 9.1%.

At this stage, the correlation coefficients between prostate volume and anthropometric parameters were: body height, 0.18; body weight, 0.008; chest circumference, 0.16.

In the second period of childhood (approximately 8–12 years), body height ranged from 120.2 to 158.1 cm, averaging 141.5 ± 0.95 cm, with a growth rate of 28.9%. Body weight varied between 20.5 and 48.4 kg, with a mean of 33.1 ± 0.70 kg, reflecting a 54.7% increase. Chest circumference at rest ranged from 55.2 to 74.5 cm, averaging 65.9 ± 0.48 cm, corresponding to a growth rate of 16.8%.

At this age, the correlation coefficients (r) between prostate volume and anthropometric indicators were: body height, 0.26; body weight, 0.05; chest circumference, 0.18.

During adolescence, body height ranged from 141.2 to 175.0 cm, with a mean of 162.3 ± 0.78 cm, corresponding to a growth rate of 14.7%. Body weight varied between 34.1 and 61.0 kg, averaging 47.6 ± 0.62 kg, reflecting a growth rate of 43.8%. Chest circumference at rest ranged from 65.0 to 80.1 cm, with a mean of 69.0 ± 0.35 cm, corresponding to a growth rate of 4.7%.

At this stage, the correlation coefficients (r) between prostate volume and anthropometric parameters were: body height, 0.02; body weight, 0.11; chest circumference, 0.14.

In late adolescence, body height varied from 154.0 to 180.0 cm, averaging 176.7 ± 0.80 cm, with a growth rate of 8.9%. Body weight ranged from 45.0 to 80.2 kg, with a mean of 65.6 ± 1.0 kg, reflecting a 37.8% increase. Chest circumference at rest was 67.0-93.2 cm, averaging 76.5 ± 0.78 cm, corresponding to a growth rate of 10.9%.

At this stage, the correlation coefficients between prostate volume and anthropometric parameters were: body height, 0.25; body weight, 0.25; chest circumference, 0.19.

In men of the first period of mature age (22–35 years), body height ranged from 156.2 to 184.0 cm, with a mean of 179.4 \pm 1.36 cm, showing a growth rate of 1.5%. Body weight varied from 48.0 to 84.1 kg, averaging 72.3 \pm 1.77 kg, reflecting a

growth rate of 10.2%. Chest circumference ranged from 68.4 to 95.0 cm, with a mean of 80.2 ± 1.3 cm, corresponding to a growth rate of 4.8%.

At this age, the correlation coefficients (r) between prostate volume and anthropometric parameters were: body height, 0.006; body weight, 0.37; chest circumference, 0.20.

In men of the second period of mature age (36–59 years), body height ranged from 158.0 to 182.4 cm, with a mean of 179.0 ± 1.78 cm, corresponding to a growth rate of 0.1%. Body weight varied from 50.4 to 86.8 kg, averaging 75.8 ± 1.78 kg, reflecting a growth rate of 4.8%. Chest circumference at rest ranged from 69.9 to 96.0 cm, with a mean of 81.7 ± 1.28 cm, showing a growth rate of 1.9%.

At this stage, the correlation coefficients (r) between prostate volume and anthropometric parameters were: body height, 0.27; body weight, 0.28; chest circumference, 0.26.

In elderly men (60–74 years), body height ranged from 152.4 to 178.0 cm, with a mean of 176.4 ± 1.25 cm, representing a decrease of 1.45% compared to the previous age group. Body weight varied from 49.0 to 81.3 kg, averaging 72.4 ± 1.58 kg, reflecting a decrease of 4.49%. Chest circumference ranged from 66.4 to 92.0 cm, with a mean of 78.6 ± 1.25 cm, representing a 3.79% reduction compared to the previous age.

At this stage, the correlation coefficients (r) between prostate volume and anthropometric parameters were: body height, 0.06; body weight, 0.20; chest circumference, 0.33.

In men of advanced age (75–90 years), body height ranged from 153.0 to 173.5 cm, with a mean of 172.0 ± 1.0 cm, representing a 2.5% decrease compared to the previous age group. Body weight ranged from 48.2 to 77.0 kg, averaging 68.2 ± 1.4 kg, reflecting a 5.8% reduction. Chest circumference fluctuated from 62.8 to 88.0 cm, with a mean of 73.0 ± 1.23 cm, showing a 7.1% decrease compared to the previous age group (see Table 6.1.1).

At this age, the correlation coefficients (r) between prostate volume and anthropometric parameters were: body height, 0.07; body weight, 0.003; chest circumference, 0.06.

Table 6.1.1.

Morphometric indices of physical development of males in postnatal ontogenesis

parameters	body growth	weight	chest
age	(cm)	body (kg)	circumference
			(cm)
newborns	46.1-53.2	3.5-4.3	34.2-43.1
	51.6±0.43	4.0±0.05	37.8±0.54
infancy	68.4-75.3	8.4-11.1	47.1-51.4
	72.0±0.39*	9.6±0.15*	49.5±0.25*
early	79.6-92.6	12.4-16.3	48.6-55.8
childhood	87.8±0.47*	14.3±0.14*	51.7±0.26*
I - childhood	94.3-124.2	13.4-31.3	50.3-61.8
period	109.8±0.78*	21.4±0.47*	56.4±0.30*
II - childhood	120.2-158.1	20.5-48.4	55.2-74.5
period	141.5±0.95*	33.1±0.70*	65.9±0.48*
adolescence	141.2-175.0	34.1-61.0	65.0-80.1
	162.3±0.78*	47.6±0.62*	69.0±0.35*
adolescence	154.0-180.0	45.0-80.2	67.0-93.2
	176.7±0.80*	65.6±1.0*	76.5±0.78*
I – the period of	156.2-184.0	48.0-84.1	68.4-95.0
mature age	179.4±1.36	72.3±1.77	80.2±1.3
II - the period of	158.0-182.4	50.4-86.8	69.8-96.0
mature age	179.0±1.78	75.8±1.78	81.7±1.28
old age	152.4-178.0	49.0-81.3	66.4-92.0
	176.4±1.25	72.4±1.58	78.6±1.25

old age	153.0-173.5	48.2-77.0	62.8-88.0	
	172.0±1.0	68.2±1.4	73.0±1.23	

Note: * - significance of differences in relation to the previous age $(P \le 0.05)$.

6.2-§. Morphometric characteristics of physical development indicators in chronic alcoholism

Anthropometric analysis demonstrated that in men of the first period of adulthood (22–35 years) with chronic alcohol consumption, body height ranged from 153.0 to 180.5 cm, with a mean value of 176.0 ± 1.35 cm. Compared to an agematched control group, this parameter exhibited a reduction of 1.9%. Body mass varied between 46.1 and 80.0 kg, averaging 69.2 ± 1.66 kg, representing a 4.3% decrease relative to controls. Resting chest circumference ranged from 64.0 to 90.7 cm, with a mean of 77.0 ± 1.3 cm, corresponding to a 4.0% reduction compared with the control cohort.

Similarly, in men of the second period of adulthood (36–59 years) affected by chronic alcohol intake, body height ranged from 154.0 to 179.4 cm, averaging 175.1 \pm 1.24 cm, which is 2.2% lower than the respective control group. Body weight fluctuated between 47.0 and 79.4 kg, with a mean of 71.0 \pm 1.59 kg, reflecting a 6.3% decrease relative to controls. Resting thoracic circumference varied from 65.2 to 90.0 cm, averaging 76.4 \pm 0.22 cm, indicating a 6.5% reduction compared to the control subjects.

The investigation revealed that in elderly men with a history of chronic alcohol consumption, stature ranged from 149.7 to 168.0 cm, with a mean of 167.0 ± 0.89 cm. Relative to an age-matched control group, this parameter exhibited a 2.9% reduction. Body mass in this cohort varied between 44.0 and 73.2 kg, averaging 62.2 \pm 1.4 kg, corresponding to an 8.8% decrease compared with controls. Thoracic

circumference at rest ranged from 59.2 to 84.0 cm, with a mean of 67.0 ± 1.21 cm, reflecting an 8.2% decline relative to the control group (see Table 6.2.1).

Table 6.2.1.

Morphometric indices of physical development of men suffering from chronic alcoholism

parameters	height	weight	chest
age	(cm)	body (kg)	circumference
			(cm)
I – the period of	153.0-180.5	46.1-80.0	64.0-90.7
mature age	176.0±1.35	69.2±1.66	77.0±1.3
II - the period of	154-179.4	47.0-79.4	65.2-90.0
mature age	175.1±1.24	71.0±1.59	76.4±0.22*
old age	149.7-168.0	44.0-73.2	59.2-84.0
	167.0±0.89*	62.2±1.4*	67.0±1.21*

Note: * - significance of differences in relation to control (P \leq 0.05).

CONCLUSION

Throughout postnatal development, the rat prostate maintains a consistent anatomical position within the pelvic cavity, situated beneath the urinary bladder and anterior or superior to the pubic symphysis. The gland overlays the urethra anteriorly, exhibits a pale pink hue, and has a soft, pliable texture. Observations indicate that both the color and consistency of the prostate remain stable with age.

In neonates and six-day-old rats, the prostate consistently presents a longitudinal-oval shape in all cases. By 11 days of age, the gland retains a longitudinal-oval form in 72.2% of animals, while 27.8% display a rounded morphology. These two morphological variants persist until approximately three months of age, at which point the prevalence of the longitudinal-oval shape rises to 83.3%, and the rounded form diminishes to 16.7%. Beginning at six months, the prostate exhibits either a bilobed structure (78.6%) or a quadrilobed configuration (21.4%).

In the bilobed arrangement, both lobes are elongated and oval, oriented longitudinally. This form of the gland lies beneath the bladder, envelops the proximal segment of the vas deferens, and extends along the lateral walls of the urethra. In the quadrilobed form, the organ comprises four distinct paired lobes, classified according to their anatomical relationship to the bladder as ventral, dorsal, lateral, and anterior lobes. The ventral lobe consists of two oval components positioned ventrolaterally relative to the bladder. The lateral and dorsal lobes, collectively referred to as the dorsolateral prostate, are aligned parallel to the urethra, situated posterior to the bladder and seminal vesicles, with their posterior surfaces adjacent to the descending colon. Both lobes lie above the superior border of the pubic symphysis. The anterior lobes, or coagulating glands, are elongated tubular structures attached along the lesser curvature of the seminal vesicles.

By nine months of age, the bilobed configuration decreases in frequency to 16.7%, whereas the quadrilobed form becomes predominant at 83.3%. In rats aged one to one and a half years, the prostate exclusively exhibits a quadrilobed architecture.

The available literature presents conflicting information regarding the number of lobes in the rat prostate. According to Nozdrachev A.D. and Polyakov E.L. (2001), the rat prostate is bilobed. In contrast, Sherstyuk O.A. et al. (2013), Knoblaugh S. et al. (2017), and Nascimento-Goncalves E. et al. (2018) describe the prostate as comprising four paired lobes—lateral, dorsal, ventral, and anterior. However, these studies do not specify the ages of the animals examined.

In the experimental cohort, the prostate of three-month-old juvenile rats was situated on the anterior surface of the pubic symphysis beneath the urinary bladder. A longitudinal-oval morphology was observed in 66.7% of animals, while 33.3% exhibited a round shape. By the sixth month, the gland demonstrated either a bilobed structure (83.3%) or a quadrilobed configuration (16.6%). In the bilobed form, both lobes were oblong-oval, located beneath the bladder, and extended along the lateral walls of the urethra, covering the proximal portion of the vas deferens.

In the quadrilobed configuration, the central lobes were positioned ventrally along the urethra just below the bladder, enveloping the initial segment of the urethra and forming two oval structures. The lateral ventral lobes lay beneath the seminal vesicles and coagulating glands, partially overlapping the ventral lobes and merging dorsally with the dorsal lobes. The dorsal lobes were located posterior and inferior to the bladder, below the attachment points of the seminal vesicles and coagulating glands. The anterior lobes consisted of convoluted oval-shaped tubules aligned along the lesser curvature of the seminal vesicles.

At nine months, the experimental rats exhibited a bilobed prostate in 75.0% of cases and a quadrilobed form in 25.0% of cases. By the twelfth month, the gland consistently presented a quadrilobed configuration. In 18-month-old experimental rats, 20% retained a bilobed structure, while 80% displayed a quadrilobed form, indicating a significant delay in the morphological maturation of the prostate compared to age-matched controls.

During postnatal development, rats exhibit variable rates of body weight gain. At birth, the average body weight is 5.16 ± 0.1 grams. By the age of eighteen months, body weight increases approximately 64.9-fold. The most pronounced weight gain

during the lactation period occurs at 21 days, reaching 87.2%, whereas the highest relative growth rate of 1.1 times is observed at 6 days of age. In the later postnatal period, the greatest increments in body mass are noted between three and six months, when the weight increases by 1.6 times and 92.5%, respectively. Beyond six months, body weight exhibits a gradual slowing of growth, reaching a 6.3% increase by 18 months.

In the experimental cohort, three-month-old rats weighed 75.6 ± 1.7 grams. By eighteen months, their body weight increased roughly 3.5 times. Animals exposed to chronic alcoholism demonstrated consistently lower body weight compared to controls across all age groups. The most substantial reductions were observed at three months (31.7%) and eighteen months (20.3%) of age.

Previous studies have reported inconsistent findings regarding the effect of alcohol on body weight. Ratcliffe F. (1972) noted that ethanol-treated rats exhibited lower body weight than controls, consistent with our results. Similarly, Symons M.A. and Marks V. (1975) reported that rats chronically exposed to 15% ethanol for three to ten weeks gained less weight than water-treated controls. Comparable observations were made by Klassen W.R. and Persaud N.V.T. (1978), Rivier C. and Vale W. (1983), Oliveira C. and Ferreira A.L. (1987), Salonen I. and Huhtaniemi I. (1990), and Cagnon V.H.A. et al. (2001).

Conversely, Anderson C. et al. (1989), who administered 3–5% ethanol to mice, found no significant difference in final body weight between ethanol-treated and control animals. Cagnon V.H.A. et al. (2001) similarly reported no statistically significant difference in weight gain by the 120th day of alcohol exposure. In addition, Willis B.R. et al. (1983) observed that body weight gain in ethanol-treated groups was comparable to controls, a finding that contrasts with the outcomes of our study.

In control animals, the highest average daily weight gain was observed during the entire lactation period, ranging from 15 to 20%, which aligns with the findings of Makarov V.G. et al. (2013), who reported that daily weight gain during milk feeding should typically fall between 10 and 20%. After the weaning period, a progressive

decline in daily weight gain is noted, reaching 0.56% in older age. During reproductive maturity, the mean daily weight increase is approximately 1.1%, consistent with the range of 0.15–1.5% reported by Makarov V.G. et al. (2013) for this stage.

In the experimental group, no significant differences in the average daily body weight gain were observed compared to the controls.

The organometric parameters of the prostate gland throughout postnatal ontogenesis are summarized in Table 1 and illustrated in Figure 1. The changes in prostate weight during postnatal development are irregular. The most pronounced increase in gland mass occurs at six months of age (76.5%), whereas the minimal growth is observed at eighteen months (9.8%).

Table 1
Biometric indices of the rat prostate gland during early and late postnatal ontogenesis

parameter	Number	Prostate			
	of	organ mass	thickness	width	length
age	animals	(gr)	(mm)	(mm)	(mm)
newborn-	18	0.08 ± 0.003	1.5±0.07	2.17±0.07	3.7±0.07
nye					
6-day	20	0.10±0.002*	1.9±0.06*	2.5±0.06	4.5±0.06*
11-day	18	0.13±0.004*	2.3±0.07*	3.1±0.13*	5.3±0.13*
16 days	17	0.15±0.004	2.8±0.14	3.5±0.07	6.3±0.14*
21 days	16	0.19±0.004*	3.6±0.15	4.6±0.15*	7.9±0.15*
1 month old	14	0.24±0.009*	4.3±0.08*	5.3±0.25	9.0±0.16*
3 months	12	0.34±0.01*	5.0±0.18	6.2±0.18	10.1±0.28
6 months	14	0.60±0.04*	6.7±0.25*	8.9±0.25*	13.0±0.41*
9 months	12	0.91±0.04*	7.5±0.18	15.0±0.55*	14.1±0.46
12 months	10	1.12±0.05	7.9±0.32	16.1±0.43	15.2±0.43
18 months	10	1.23±0.07	8.4±.32	17.4±0.43	16.1±0.43

Note: * - statistical significance of differences compared with the previous age ($P \le 0.05$).

The biometric characteristics of the prostate in rats from the experimental group are presented in Table 2 and illustrated in Figure 2.

In rats subjected to chronic alcoholism, a reduction in organ mass was observed across all age groups when compared with control animals. The most pronounced decreases in body weight occurred at 3 months (41.2%) and 18 months (35.0%) of the study.

The highest prostate mass coefficient was recorded in neonatal rats (1.55%). By the end of the lactation period, this parameter ranged from 0.63% to 0.92%. In the subsequent stages of life, the mass coefficient remained between 0.21% and 0.56%.

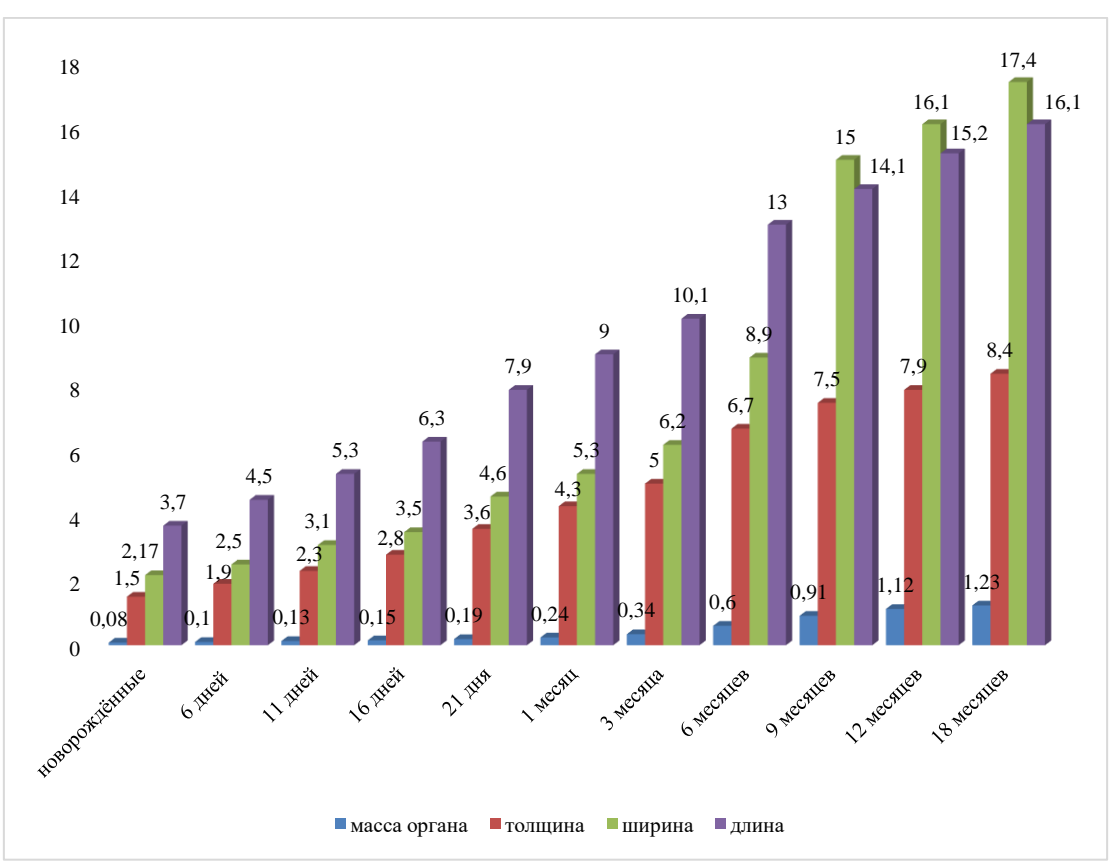


Fig. 1. Morphometric indices of the rat prostate during postnatal ontogenesis

The prostate mass coefficient in rats from the experimental group ranged between 0.24% and 0.37%. Compared with age-matched controls, a decline was observed at 6 months (17.9%) and 18 months (35.1%) of the study. In the remaining age groups, a slight increase in this parameter was noted, which aligns with the findings of Knyazkin I.V. et al. (2012), who reported no significant alterations in the mass

coefficient of the prostate and seminal vesicles in rats experiencing either acute or chronic organ inflammation.

Table 2
Morphometric parameters of the prostate of rats of the experimental group under chronic alcohol exposure

parameter	quantity	Prostate			
	animals	organ	thickness	width	length
age		mass	(mm)	(mm)	(mm)
		(gr)			
3 months	12	0.20±0.02*	4.0±0.18	5.1±0.18*	7.9±0.28*
6 months	12	0.45±0.04	5.7±0.18	8.1±0.37	11.0±0.55
9 months	8	0.85±0.06	6.5±0.27	13.4±0.8	12.2±0.67
12 months	10	1.03±0.05	7.0±0.22	15.2±0.54	13.9±0.54
18 months	10	0.80±0.05*	7.1±.22	14.4±0.54*	13.0±0.43*

Note: * - reliability of differences in relation to control (P \leq 0.05).

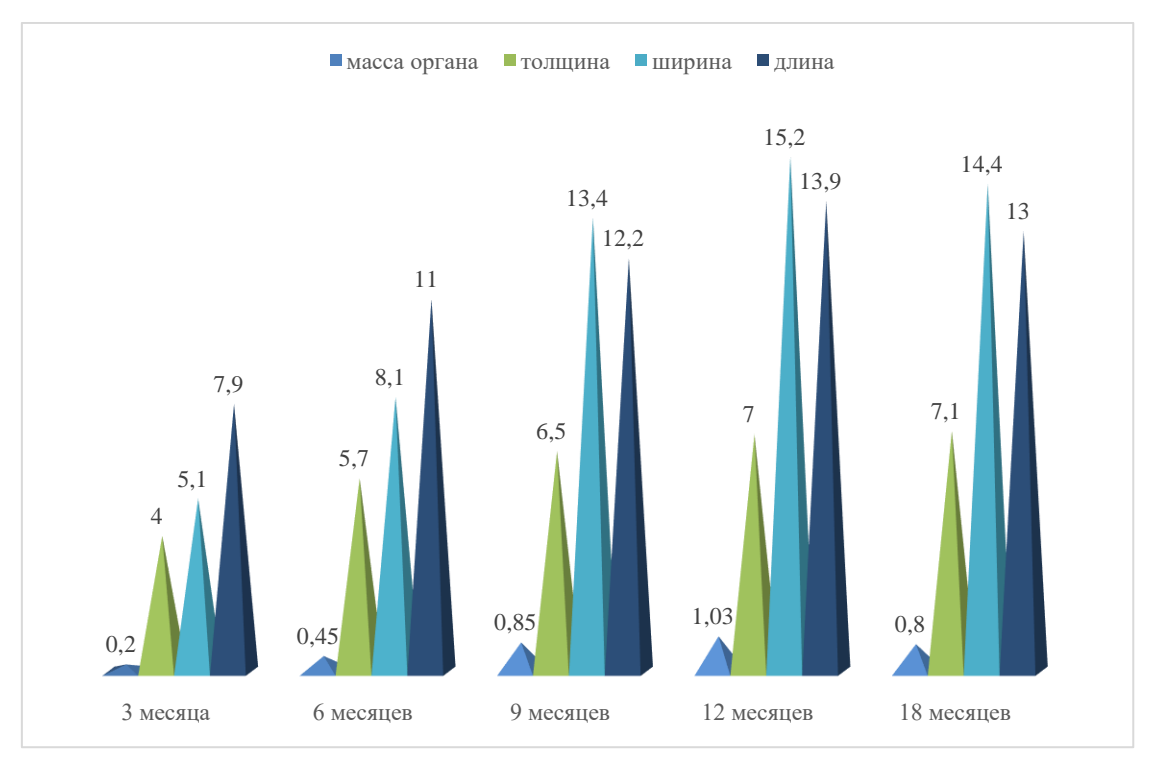


Fig. 2. Morphometric indices of the prostate of rats of the experimental group

It has been demonstrated that the linear dimensions of the prostate gland progressively increase throughout postnatal ontogenesis. Comparable findings were reported by Alekseev Yu.D. et al. (2015), who observed age-related growth in the organometric parameters of the human prostate, attributing this to gradual maturation and the establishment of the gland's structural and functional characteristics.

In newborn rats, the anteroposterior thickness of the gland measures 1.5 ± 0.07 mm, increasing 5.6-fold by 18 months of age. During the lactation period, the most pronounced increases in thickness occur on days 6 (26.7%) and 21 (28.6%) of development. In the later postnatal stages, the largest growth in anteroposterior size is observed at 1 and 6 months of age, with increases of 19.4% and 34.0%, respectively.

In the experimental group, 3-month-old rats exhibit a gland thickness of 4.0 ± 0.18 mm, which grows 1.8-fold by 18 months. Compared with controls, the anteroposterior dimension is reduced across all age groups, most notably at 3 months (20.0%) and 18 months (15.5%).

The transverse (width) dimension of the gland at birth is 2.2 ± 0.07 mm, expanding 7.9-fold by 18 months. During the suckling period, the greatest increases occur on days 11 (24.0%) and 21 (31.4%). In the later stages of postnatal development, maximal transverse growth is observed at 6 and 9 months, with increases of 43.5% and 68.5%, respectively.

In the experimental group, the transverse dimension of the prostate in juvenile rats measures 5.1 ± 0.18 mm, increasing 2.8-fold by 18 months of age. When compared with the control group, the gland's width is consistently reduced across all age groups, with the most pronounced decreases observed at 3 months (17.7%) and 18 months (17.2%).

The longitudinal (length) of the prostate in newborn rats is 3.7 ± 0.07 mm, expanding 4.4-fold by 18 months. During the early postnatal period, the greatest increases in organ length occur on days 6 (22.6%) and 21 (25.4%) of development.

At later stages, the most significant growth is observed at 1 and 6 months of age, with increases of 13.9% and 28.7%, respectively.

In the experimental animals, the organ length at 3 months is 7.9 ± 0.28 mm, which grows 1.6-fold by 18 months. Relative to controls, the longitudinal dimension of the gland is reduced at all ages, most markedly at 3 months (21.8%) and 18 months (19.3%).

It is noteworthy that, in both control and experimental groups, the longitudinal dimension remains greater than the transverse and anteroposterior sizes throughout early ontogenesis. From 9 months onward, however, the width of the prostate begins to surpass both the length and thickness of the organ.

In summary, the progression of body weight and prostate biometric parameters during postnatal development, as well as under chronic ethanol exposure, exhibits distinct patterns, largely dependent on age-related anatomical characteristics and the timing of prolonged alcohol exposure.

Ultrasonographic assessment has demonstrated that the anteroposterior (thickness) dimension of the prostate in newborn boys is 8.9 ± 0.32 mm, increasing approximately 4.0-fold by old age. The most pronounced growth in prostate thickness occurs during adolescence (38.5%), likely associated with the second pubertal growth spurt. These findings align with the observations of Kurbanov F.T. (2007), who reported a significant increase in prostate biometric parameters beginning at 11–15 years of age. Filippova E.A. (2008) similarly noted rapid prostate enlargement around 13–14 years. Conversely, the slowest growth is observed during infancy (5.6%) and in elderly men (2.0%), consistent with Esakov S.A. (2010), who emphasized minimal prostate growth in newborns and during the first year of life.

The transverse (width) dimension of the prostate expands 9.7-fold from the neonatal period (4.8 ± 0.22 mm) to old age (46.5 ± 0.27 mm). The largest increase occurs in adolescence, where the width doubles, while the smallest growth is seen in elderly men (3.1%). This finding contrasts with Filippova E.A. (2008), who suggested that the prostate gradually narrows transversely after 45 years of age.

The longitudinal (length) dimension of the prostate in newborn boys is 9.8 ± 0.32 mm, increasing 3.9-fold by old age. The fastest growth in length is observed during adolescence (34.0%) and in early childhood (4–7 years, 21.4%), which correlates with Esakov S.A. (2010) indicating that early childhood corresponds to a noticeable enlargement of the prostate, likely due to the first growth spurt. The least increase in longitudinal size is recorded in elderly men (2.7%).

It should be noted that until the second period of childhood, the length of the gland is greater than its width and thickness. Beginning in adolescence, the transverse size is observed to prevail over the longitudinal and anteroposterior parameters, which is inconsistent with the data of Ivanchenko O.F. (1994), according to whom this prevalence is observed in children aged 6-9 years.

The study demonstrated that the prostate gland volume at birth is 0.24 ± 0.02 cm³, increasing approximately 136.3-fold by old age (32.7 ± 0.81 cm³). The most substantial growth occurs during adolescence, with prostate volume expanding 3.4-fold, likely reflecting the pubertal growth spurt. Conversely, the slowest volumetric increase is observed in elderly men (7.9%).

It is important to note that there remains no universally accepted consensus regarding sonographic reference values for the prostate. Several studies report differing linear and volumetric parameters, often without specifying the ages of the subjects examined, which complicates direct comparison of organometric data across investigations.

Author	Dimensions, cm			
Author	Thickness	Width	Height	
Watanabe H. et al., 1974	2.76±0.4	4.8±0.4	2.8±0.5	
watanaoc 11. ct al., 1974	(2.1-3.4)	(3.9-5.3)	(2.0-4.0)	
Demidov V.N. et al., 1989	1.8-2.5	2.7-4.2	2.5-4.0	
Penu A.Yu., 1990	1.5-2.5	2.4-4.0	2.3-3.8	
Ignashin N.S., Vinogradov V.R., 1990	1.6-2.3	2.7-4.3	2.4-4.3	
Lavrova S.A., Tkachenko P.M., 1999	1.8-2.4	2.7-4.5	2.4-4.1	

Hofer M., 2002	< 3	< 5	< 3
Kapustin S.V., Pimanov S.I., 2005	1.7-2.3	2.2-5.0	2.5-4.2
Filippova E.A., 2008	1.7-2.5	3.5-5	3.2-4.5
Nazarenko G.I., Khitrova A.N., 2017	2.5	3.5	4.0

Historically, there has been considerable disagreement in the literature regarding the volumetric parameters of the prostate gland. Watanabe H. et al. (1974) reported an average normal prostate volume of 21.0 ± 5.6 cm³. Ignashin N.S. and Vinogradov V.R. (1990) suggested that normal volume should remain below 24 cm³, while Cooner W.H. et al. (1994) proposed a maximum of 20 cm³. Lavrova S.A. and Tkachenko P.M. (1999) indicated that the volume should not exceed 20 cm³, Hofer M. (2002) suggested <25 cm³, and Kapustin S.V. and Pimanov S.I. (2005) estimated it at approximately 25 cm³. Zubarev A.V. and Gazhonova V.E. (2002) reported a wider range of 20–30 cm³, whereas Sholokhov V.N. et al. (2006) noted that prostate volume could fluctuate between 20 and 40 cm³ depending on age. The most recent data by Trufanova G.E. and Ryazanova V.V. (2016) indicate that the upper physiological limit of prostate volume in men may reach 40 cm³, with values above this threshold being considered hypertrophic.

In men with chronic alcoholism, the anteroposterior dimension of the prostate increases by 29.8% from the first period of mature age to old age. Specifically, compared with age-matched controls, the anteroposterior size is enlarged by 13.8% in the first period of middle age, 3.8% in the second period, and 17.4% in elderly men. The transverse dimension of the gland also expands by 30.5% over the same age span, with increases relative to controls of 6.1%, 1.0%, and 10.0% at the first, second, and elderly age periods, respectively.

In men with chronic alcoholism, the longitudinal dimension of the prostate increases by 27.8% from the first period of mature age to old age. When compared with age-matched controls, the longitudinal size is elevated by 33.6% in the first stage of middle age, 28.6% in the second stage, and 27.2% in elderly men.

Prostate volume in individuals with chronic alcoholism rises 2.2-fold across the same age span. Relative to the control group, this parameter increases by 61.3% in the first stage of middle age, 35.1% in the second stage, and 64.0% in elderly men.

Anthropometric analysis has shown that in newborn boys, body height averages 51.6 ± 0.43 cm, increasing approximately 3.3 times by old age. The most rapid growth occurs during infancy, with an increase of 39.5%. Notably, body height gradually declines starting from the second period of mature age, with the most significant reduction observed in elderly men (2.5%).

At birth, the correlation coefficient between body height and prostate volume is 0.35. In other age groups, it ranges from 0.02 to 0.27, with the exception of the first period of adulthood (0.006), where no significant correlation is observed.

The study also found that newborn body weight averages 4.0 ± 0.05 kg and increases 17.1-fold by old age. The highest growth occurs in infancy, with a 2.4-fold increase. In elderly and old men, body weight declines, most prominently in old age (5.8%).

The strongest correlation between body weight and prostate volume is observed in the first period of mature age (0.37). In other age groups, the correlation ranges from 0.05 to 0.28, except for the first period of childhood (0.008) and old age (0.003), where no correlation is detected.

Chest circumference in newborn boys averages 37.8 ± 0.54 cm, increasing approximately 1.9-fold by old age. The most rapid growth occurs during infancy, with a rise of 31.0%. In elderly and old men, chest circumference gradually declines, with the most pronounced reduction observed in old age (7.1%).

At birth, the correlation coefficient between chest circumference and prostate volume is 0.55. In other age groups, this correlation varies between 0.06 and 0.33.

In men with chronic alcoholism, body height decreases by 5.1% from the first period of mature age to old age. When compared to age-matched controls, body height is reduced by 1.9% in the first stage of middle age, 2.2% in the second stage, and 2.9% in elderly men.

Body weight in chronic alcoholics declines by 10.1% across the same age span. Relative to the control group, weight decreases by 4.3% in the first stage of middle age, 6.3% in the second stage, and 8.8% in old age.

Chest circumference in men affected by chronic alcoholism diminishes by 13.0% from the first period of mature age to old age. Compared with controls, this parameter decreases by 4.0% in the first stage of middle age, 6.5% in the second stage, and 8.2% in elderly men.

Thus, based on the findings of the study, the following conclusions can be drawn:

- 1. **Prostate Morphology in Rats:** In white rats, the prostate exhibits a round or longitudinal-oval shape from birth to 6 months of age. Between 6 and 12 months, the gland develops a two- or four-lobed structure, which becomes exclusively four-lobed from 12 to 18 months. During the first 9 months, the longitudinal dimension exceeds both the transverse and anteroposterior sizes; from the 9th month onward, the width surpasses the length and thickness. In the experimental group, a marked delay in both the morphological development and the growth of the prostate gland is observed compared to controls.
- 2. Effects of Chronic Alcoholism on Rats: Rats exposed to chronic alcohol consumption demonstrate deficits in body weight, prostate mass, and linear dimensions of the gland across all age groups, with the most pronounced reductions at 3 months and 18 months of age. Average daily body weight gain remains largely unchanged relative to controls. The prostate mass coefficient in the experimental group ranges from 0.24% to 0.37%, showing significant reductions in the 6th month (17.9%) and 18th month (35.1%), while other age periods exhibit minor increases.
- 3. **Prostate Development in Humans:** During postnatal development, ultrasonography reveals progressive increases in the linear and volumetric parameters of the prostate. The greatest growth in length occurs during adolescence (34.0%), while thickness increases by 38.5%, width doubles,

and gland volume expands 3.4-fold. The smallest gains in size are observed in elderly men. Up to the second period of childhood, the longitudinal dimension predominates over both transverse and anteroposterior sizes; from adolescence onward, the width of the gland becomes the largest dimension.

- 4. **Prostate Changes in Chronic Alcoholism:** In men with chronic alcoholism, the prostate gland demonstrates an increase in volumetric and linear dimensions. Relative to the control group, the most pronounced increase in longitudinal size occurs during the second period of mature age (28.7%), while the largest gains in transverse size (10.0%), anteroposterior thickness (17.4%), and overall gland volume (64.0%) are observed in elderly men.
- 5. **Anthropometric Development Across Lifespan:** The most substantial growth in body height, weight, and chest circumference is observed during infancy, whereas elderly and older men exhibit slight declines in these parameters. In individuals affected by chronic alcoholism, there is a noticeable delay in the development of anthropometric indices compared with controls, with the most significant deficits evident in old age.
- 6. Correlation Between Prostate Volume and Physical Development: The study revealed weak to moderate positive correlations between prostate volume and anthropometric parameters across all age groups: height (r = 0.02-0.35), body weight (r = 0.05-0.37), and chest circumference (r = 0.06-0.55).

LIST OF USED LITERATURE

- 1.Абоян И.А., Толмачев А.Н., Лемешко С.И. Морфологическая характеристика ткани гиперплазии предстательной железы при хроническом простатите // Экспериментальная и клиническая урология. 2020. №4. с.38-46.
- 2.Алексеев Ю.Д., Савенкова Е.Н., Ефимов А.А., Райкова К.А. Сравнительный анализ органометрических показателей мужских половых желез человека в различные возрастные периоды // Бюллетень медицинских Интернет-конференций (ISSN 2224-6150) 2015.- Том 5. № 7. С. 993-996.
- 3.Аляев Ю.Г. Урология. Российские клинические рекомендации. М.: ГЭОТАР-Медиа. 2018. 456 с.
- 4.Батуева А. Б. Гистологическое строение предстательной железы серебристо-черных лисиц и содержание в ней углеводных компонентов / А. Б. Батуева. Текст: непосредственный // Морфология. 2000. Т.117. №3. С. 19-28.
- 5.Боровская Т. Г. Состояние сперматогенеза крыс после введения противоопухолевого препарата паклитаксела / Т. Г. Боровская, В.Е. Гольдберг, О.А. Румпель и др. // Бюллетень экспериментальной биологии и медицины. 2009. Том 147. № 6. С. 655-658.
- 6.Будник А.Ф., Богатырёва О.Е., Мусукаева А.Б. Морфологическая характеристика простаты человека при хронической алкогольной интоксикации // Международный научно-исследовательский журнал. 2016. № 3 (45). С. 50-52.
- 7.Громов А.И., Капустин В.В., Прохоров А.В. Зональная анатомия предстательной железы: всегда ли нам нужна центральная зона? //

- Медицинская визуализация. -2017. № 21 (1). С. 69–74. DOI: 10.24835/1607-0763-2017-1-69-74.
- 8. Демидов В.Н., Пытель Ю.А., Амосов А.В. Ультразвуковая диагностика в уронефрологии. М., Медицина, 1989, 105 с.
- 9. Есаков С.А. Возрастная анатомия и физиология (курс лекций) / УдГУ. Ижевск, 2010. -196 с.
- 10.Задонская В. Ю. Гистологические особенности предстательной железы самцов американской норки / В. Ю. Задонская. Текст: электронный // Материалы научно-практической конференции молодых ученых «Инновационные идеи молодых исследователей для агропромышленного комплекса России» (29-30 марта 2018 года) / Министерство сельского хозяйства [и др.]. Пенза: Пензенский государственный аграрный университет, 2018. С. 45-48.
- 11.Западнюк В.И. К вопросу о возрастной периодизации лабораторных животных // Старение клетки. Киев, 1971. С. 433-438.
- 12.Западнюк И.П., Западнюк В.И., Захария Е.А. Лабораторные животные. Разведение, содержание, использование в эксперименте. Киев: Выща школа. 1983. 383 с.
- 13.Захаров А.А. Особенности морфометрических показателей предстательной железы неполовозрелых крыс после применения иммуносупрессора // Вестник Смоленской государственной медицинской академии. 2017. Т. 16. № 4. С. 12-18.
- 14.Зубарев А.В., Гажонова В.Е. Диагностический ультразвук. Уронефрология. - М., 2002. - С. 147-150.
- 15.Иванец Н.Н., Анохина И.П., Винникова М.А. Наркология. Национальное руководство. М.: ГЭОТАР - Медиа. – 2016. - 944 с.

- 16.Иванченко О.Ф. Возможности эхографии в диагностике нарушения формирования пола у детей: автореф. дис. ... канд. мед. наук / Иванченко О.Ф. М.: РМАПО, 1994. 22 с.
- 17.Игнашин Н.С., Виноградов В.Р. Трансректальное ультразвуковое исследование предстательной железы и семенных пузырьков. // Методические рекомендации. М. 1990. 38 с.
- 18. Капустин С.В., Пиманов С.И. Ультразвуковое исследование в таблицах и схемах, Витебск, 2005. 64 с.
- 19.Кащенко С.А., Захаров А.А. Особенности морфоструктуры предстательной железы и семенных пузырьков животных периода выраженных старческих изменений при циклофосфамид-индуцированной иммуносупрессии // Крымский журнал экспериментальной и клинической медицины. Том:8, № 3, 2018, С. 35-42. УДК: 611.659.084:615.37.
- 20.Кнышёва Л.П. и др. Критерии достоверности воспроизведения экспериментальной модели хронической алкогольной интоксикации // Волгоградский научно-медицинский журнал. 2016. №4. С. 48-51.
- 21.Князькин И.В., Горбачев А.Г., Аль-Шукри С.Х., Боровец С.Ю., Тюрин А.Г. Патогенетическая модель простатита в эксперименте на мелких лабораторных животных // Нефрология. 2012. Том 16. №3 (выпуск 1). С. 109-113 ISSN 1561-6274.
- 22.Коптяева К.Е., Мужикян А.А., Гущин Я.А., Беляева Е.В., Макарова М.Н., Макаров В.Г. Методика вскрытия и извлечения органов лабораторных животных // Сообщение 1: крыса. Лабораторные животные для научных исследований. 2018. №2. С. 71-92. DOI: 10.29296/ 10.29296/2618723X-2018-02-08.

- 23. Курбанов Ф.Т. Основы ультразвуковой волюмометрии (руководство для практических врачей). Под редакцией профессора А.А. Фазылова. Ташкент. 2007. 63 с.
- 24. Лаврова С. А., Ткаченко П. М. Ультразвуковая диагностика заболеваний предстательной железы // Журнал Новости лучевой диагностики. 1999. № 1. С. 11-14.
- 25.Ланина В.А., Химичева М.Н., Кузьменко В.В. и др. Хронобиологические особенности больных с хроническим простатитом при аденоме простаты // Тенденции развития науки и образования. — 2020. - №66(1). - C.111—114.
- 26.Лугин И. А., Троценко Б. В. Развитие простатита при гипокинетическом стрессе // Современная медицина: Актуальные вопросы. 2014. № 37. С. 47-80. ISSN: 2309-3552.
- 27. Макаров В.Г., Макарова М.Н., Абрашова Т.В., Гущин Я.А., Ковалева М.А., Рыбакова А.В., Селезнева А.И., Соколова А.П., Ходько С.В. Справочник. Физиологические, биохимические и биометрические показатели нормы экспериментальных животных. СПБ.: Изд-во «ЛЕМА», 2013.- 116 с.
- 28.Мухотрофимова О.М. Сравнительная морфофункциональная характеристика органов размножения некоторых видов грызунов (RODENTIA): автореф. дисс. ... канд. биол. наук / Мухотрофимова О.М. Москва, 2010, 21с.
- 29. Назаренко Г.И., Хитрова А.Н. Ультразвуковая диагностика предстательной железы в современной урологической диагностике. Видар, 2017. 304 с.
- 30.Нефедченко А.В., И.В.Наумкин. Спланхнология домашних животных: система органов размножения: учеб. метод. пособие / Новосиб. гос. аграр. ун-

- т, ГНУ ИЭВСиДВ Россельхозакадемии; Новосибирск: Изд-во НГАУ, 2012. 101с.
- 31.Неймарк А.И. и др. Патоморфологические изменения предстательной железы при вибрационной болезни //БЮЛЛЕТЕНЬ СО РАМН 2008. № 6 (134). С. 145-150.
- 32.Никитин, А.И. Вредные факторы среды и репродуктивная система человека (ответственность перед будущими поколениями) / А.И.Никитин. СПб.: Эл-би-СПб, 2005. 216 с.
- 33. Ноздрачёв А.Д., Поляков Е.Л. Анатомия крысы (Лаборат. животные) / Под ред. академика А.Д. Ноздрачёва. СПб.: Издательство «Лань», 2001. 464 с.
- 34.Островская Т. А. Сравнение макроанатомии простаты человека и лабораторных животных / Т. А. Островская, А. К. Усович // Достижения фундаментальной, клинической медицины и фармации: (тез. докл. 59-й науч. сес. ун-та, посвящ. 70-летию ВГМУ, 26-27 февр. 2004 г.). Витебск, 2004. С. 16.
- 35.Петько И. А., Усович А. К. Формирование и преобразование желёз простаты человека в пренатальном и неонатальном периодах // Онтогенез. 2019, том 50. № 2. С. 141–146.
- 36.Пену А.Ю. Практическая эхография: атлас / Кишинев: Штиинца, 1990. 286 с.
- 37.Рыбакова А.В. Методы эвтаназии лабораторных животных в соответствии с европейской директивой 2010/63 / А.В. Рыбакова, М.Н. Макарова // Международный вестник ветеринарии. 2015. №2. С. 96-107.
- 38. Савельева А.Ю. Практикум по анатомии декоративных и экзотических животных [Электронный ресурс] / А.Ю. Савельева; Краснояр. гос. аграр. ун-т. Красноярск, 2018. 284 с.

- 39.Саяпина И.Ю., Целуйко С.С., Лашин С.А., Остронков В.С. Функциональная морфология органов мужской репродуктивной системы при адаптации к низким температурам на фоне коррекции дигидрокверцетином. Монография. Благовещенск: ООО «Типография». 2018. 179 с.
- 40.Сидоров П.И. Использование лабораторных животных в токсикологическом эксперименте: методические рекомендации. Под ред. Сидорова П.И. Архангельск. 2002. 15 с.
- 41.Степанова Э.Ф., Евсеева М.М., Карагулов Х.Г. Применение свечей «тамбуил» у крыс с интерстициальным простатитом (экспериментальное исследование) // Научные ведомости Серия Медицина. Фармация. 2011.- № 22 (117). Выпуск 16/2. С. 35-38.
- 42. Теленков В. Н. Сравнительная морфология предстательной железы у пушных зверей клеточного содержания: дисс ... канд. вет. наук: 16.00.02 / Теленков В. Н. Омск, 2001.- 193 с.
- 43. Теленков В.Н. Морфофункциональные особенности органов мочеполового аппарата самцов у представителей отрядов хищных и зайцеобразных: дисс. ... докт. вет наук: 16.00.02 / Теленков В. Н. Омск, 2022, 325 с.
- 44. Труфанов Г.Е., Рязанов В.В. Практическая ультразвуковая диагностика. Руководство в 5-ти томах. Том 2. Издательство: ГЕОТАР-МЕДИА, 2016 г.- 198 с.
- 45.Хныкин Ф. Н. Топографо-анатомические особенности простаты и ее экстраорганных сосудов у взрослого человека: автореф. дисс. ... канд. мед. наук / Хныкин Ф. Н. Санкт-Петербург, 2005 г. 18 с.
- 46.Хорош В.Я., Мысак А.И. Экспериментальное цитотоксическое поражение предстательной железы в моделировании хронического

- простатита// Экспериментальная и клиническая урология. 2013. №2. С. 35-37.
- 47.Хофер М. Компьютерная томография. Базовое руководство. 2-е издание, переработанное и дополненное: М.: Мед. лит., 2008. 224 с. ISBN 978-5-89677-121-0.
- 48.Филиппова Е.А. Ультразвуковая диагностика заболеваний предстательной железы у детей // Вестник РНЦРР Минздрава России. 2008. №8. С. 27-46.
- 49. Устенко Р. Л. Стереоморфологические особенности желез периферической зоны простаты человека / Р. Л. Устенко, О. А. Шерстюк, Н. Л. Свинцицкая [и др.] // Таврический медико-биологический вестник. 2013. Т. 16, № 1, Ч. 2 (61). С. 193-197.
- 50.Цветков И. С. Структурно-функциональные изменения предстательной железы и органов иммунной системы крыс вистар при хроническом аутоиммунном воспалении в условиях нормо и гиперандрогенемии: автореф. дисс. ... канд. биол. наук / Цветков И. С. Москва, 2012. 26 с.
- 51.Цыдыпов Р.Ц. Морфология и гистохимия предстательной железы сельскохозяйственных животных в сравнении // Mongolian Journal of Agricultural Sciences. 2014. №13 (02). С. 29-32.
- 52. Шамирзаев Н.Х., Тухтаназарова Ш.И. и Тен С.А. Морфометрическая характеристика оценки физического развития детей и подростков // Методические рекомендации. Ташкент, 1998. 16 с.
- 53. Шарыпова Н.В. Концентрация гормонов, регулирующих половую функцию, при длительном воздействии стресс-факторов чрезвычайной интенсивности / Н.В. Шарыпова, А.А. Свешникова // Фундаментальные исследования. 2013. № 3. С. 404-410.

- 54.Шерстюк О.А. и др. Роль анатомических знаний в диагностике и лечении заболеваний простаты // Вісник проблем біологіі і медицини. 2013. Т.2, №3. С. 56-61. [Sherstjuk O.A. i dr. Visnyk problem biologii i medycyny. Bulletin of Biology and Medicine. 2013. Т.2, №3. Р. 56-61. (in Russian).
- 55.Шолохов В.Н., Бухаркин Б.В., Лэпэдату П.И. Ультразвуковая томография в диагностике рака предстательной железы. 1-е издание М.: ООО «Фирма СТРОМ», 2006. 112 с.
- 56. Юров М. А. Структурные изменения простаты и лимфатических узлов при моделировании алкогольной интоксикации в сочетании с венозным застоем и фитокоррекцией: автореф. дисс. ... канд. мед. наук / Юров М. А. Новосибирск, 2012 год. 28 с.
- 57.Adam Cox, Matthew Jefferies, Raj Persad, Prostate Structure and Function, Blandy's Urology, 10.1002/9781118863343, (509-521), (2019).
- 58.Adebayo A., Akinloye A., Olukole S., Ihunwo A., Oke B. Anatomical and immunohistochemical characteristics of the prostate gland in the greater cane Rat (Thryonomys swinderianus). Anatomia, Histologia, Embryologia. 2014. 1-8 doi: 10.1111/ahe.12122.
- 59.Akbari G., Babaei M., Kianifard D., Mohebi D. (2018) The gross anatomy of the male reproductive system of the european hedgehog (Erinaceus Europaeus) // Folia Morphol. Vol.77. No.1, P. 36–43.
- 60.Akbari G., Kianifard D. (2017). Anatomy, Histology and Histochemistry of Accessory sex glands in male Persian squirrel (Sciurusaomalus) // Italian Journal of Anatomy and Embryology, 122: 17-26.
- 61.<u>Alsafy M.M.A., Abumandour A.A.K., El-Bakary R., Seif M.A., Roshdy K.</u> Morphological examination of the accessory sex glands of the Barki bucks (Capra hircus) // Folia Morphol. (Warsz). 2021. Jun 1. P. 28-39.

- 62.Bannowsky A. Two years follow-up after nerve-sparing radical prostatectomy -improvement of erectile function with nightly low dose sildenafil / A. Bannowsky, H. Schulze, C. Van der Horst [et al.] // AUA. 2088. 1250 p.
- 63.Barone R. (2001). Splanchnologie II. In: Anatomie comparée des mammifères domestiques. Tome quatrième, Triosième edition, Paris, -242 p.
- 64.Berquin I., Min Y., Wu R., Wu H., Chen Y. (2005). Expression signature of the mouse prostate // J. Biol. Chem. 2005, 68-77.
- 65.Bhavsar A., Verma S. (2014). Anatomic imaging of the prostate // BioMed Research International, 2014, 1–9.
- 66.Bostwick D., Cheng L. (2014). The zonal anatomy of the prostate // Urological Surgical Pathology. –Volume 2. Issue 1. Pages 35-49.
- 67.Bosland M.C. Chemical and hormonal induction of prostate cancer in animal models // Urol. Oncol. 1996. Vol. 2. P. 103–110.
- 68.Bosland M. C., Ozten N., Eskra J., Mahmoud A. A Perspective on Prostate Carcinogenesis and Chemoprevention // Curr Pharmacol Rep. 1 (2015) 258–265.
- 69.Boorman G., Elwell M., Mitsumori K. Male accessory sex glands, penis and scrotum. In Payhology of the Fischer Rat; Boorman, G., Ed.; Academic Press: Cambridge, MA, USA, 1990. 128 p.
- 70.Borges E.M., Branco E., Lima A.R., Leal L.M., Leandro Luiz Martins L.L., Reis A.C.G., Cruz C., Machado M.R.F., Miglino M.A. (2014). Morphology of accessory genital glands of spotted paca (Agouti paca Linnaeus, 1766). Animal Reproduction Science 145:75–80.
 - 71.Brock M. et al. // J. Urol. 2018; 187:2039-2043.
- 72.Buskin A., Singh P., Lorenz O., Robson C., Douglas W. S., Heer R. A. Review of Prostate Organogenesis and a Role for iPSC-Derived Prostate Organoids

- to Study Prostate Development and Disease // International Journal of Molecular Sciences, 10.3390 /ijms 222313097, 22, 23, (13097), (2021). P. 78-86.
- 73.Budras K.D., Habel R.E., Wunsche A., Buda S. Bovine anatomy: An illustrated text. 1st ed. Schlutersche GmbH & Co. KG, Verlag und Druckerei, Hannover 2003: 289–291.
- 74.Cagnon V.H.A., Garcia P.J Martinez F.E. Martinez M. and Padovani C.R. 1996. Ultrastructural study of the coagulating gland of wistar rats submitted to experimental chronic alcohol ingestion // The Prostate., 28, 341-346.
- 75.Cagnon, V.H.A., Garcia, P.J., Guazzelli Filho, J., Martinez, F.E., Mello, Jr. W. and Martinez M. 1998. Ultrastructural study of the lateral lobe of the prostate of Wistar rats submitted to experimental chronic alcohol ingestion // J. Submicrosc. Cytol. Pathol., 30(1), 77-84.
- 76.Cagnon V. H. A., Tomazini F. M., Garcia P. J., Martinez F. E., Martinez M., Padovani C. R. Structure and ultrastructure of the ventral prostate of isogenic mice (C57B1/6J) submitted to chronic alcohol ingestion Tissue & Cell, 2001, 33 (4) 354-360.
- 77.Calamar C.D., Patruica S., Dumitrescu G., Bura M., Dunea I.B., Nicula M. (2014). Morpho histological studies on the male genital apparatus of Chinchilla laniger. Scientific Papers Animal Science and Biotechnologies 47(1):275-280.
- 78.Candido E.M. Experimental alcoholism and pathogenesis of prostatic diseases in UChB rats / Candido E.M., Carvalho C.A., Martinez F.E. et al. // Cell Biology International. 2013. Vol. 31, № 5. P. 459-472.
- 79. Cepeda R., Adaro A., Peñailillo P. (2006) Variaciones morfometricas de la próstata de Chinchilla laniger (Molina, 1982) y de la concentración de testosterona plasmática durante un ciclo reproductivo annual // Int. J. Morphol. 24: 89-97.
- 80.Chaves E. M., Aguilera-Merlo C., Filippa V., Mohamed F., Dominguez S., and Scardapane L. 2011: Anatomical, histological and immunohistochemical study

- of the reproductive system accessory glands in male viscacha (Lagostomus maximus maximus) // Anat. Histol. Embryol. 40, 11–20.
- 81. Civenni G., Carbone G. M., Catapano C. V. (2018). Overview of genetically engineered mouse models of prostate cancer and their applications in drug discovery. Current Protocols in Pharmacology, 81(1), 39-51.
- 82.Cooner W.H. et al. Prostate cancer detection in clinical urological practicae by ultrasonography, digital rectal examination tnd speciphic antigen. // J. Urologyl. 1994. V.143. P. 1146-1154.
- 83.Creasy D., Bube A., de Rijk E., Kandori H., Kuwahara M., Masson R., Nolte T., Reams R., Regan K., Rehm S. et al. Proliferative and Nonproliferative Lesions of the Rat and Mouse Male Reproductive System // Toxicol. Pathol. 2012, 40, 40–121.
- 84.Cunha G.R., Vezina C.M., Isaacson D., Ricke W.A., Timms B.G., Cao M., Franco O., Baskin L.S. (2018) Development of the human prostate // Differentiation 103: 24–45.
- 85.Cunha G.R., Sinclair A., Ricke W. A., Robboy S. J., Cao M., Baskin L. S., Reproductive tract biology: Of mice and men // Differentiation, 10.1016/j.diff.2019.07.004, 110, (49-63), (2019).
 - 86.De Marzo A., Platz E., Sutcliffe S., Xu J., Gronberg H., Drake C. (2007).
- Inflammation in prostate carcinogenesis // Nat. Rev. Cancer. 185 (38-46) http://dx.doi.org/10.1038/nrc2090.
- 87.Diya B. J., Anne E. T., Chad M. V., Douglas W. S. Progenitors in prostate development and disease // Developmental Biology, 10.1016 / j. ydbio. 2020. 11.012, 473, (50-58), (2021).
- 88.El-Shahat A.E. Altered testicular morphology and oxidative stress induced by cadmium in experimental rats and protective effect of simultaneous green tea

- extract / A.E. El-Shahat, A. Gabr, A.R. Meki et al. // International Journal of Morphology. $-2009. \text{Vol.}\ 27, \, \text{N}\tiny{2}\ 3. \text{P.}\ 757-764.$
- 89.Evans H. E., de Lahunta A. Mıller's Anatomy of the Dog. 4nd edition. WB Saunders Company. Philadelphia, London, Sydney, Tokyo. 2013: 1062–1067. ISBN: 978-143770812-7.
- 90.Fabiane F. Martins, Mateus R. Beguelini, Cintia C.I. Puga, Eliana Morielle-Versute, Patricia S.L. Vilamaior, Sebastiao R. Taboga, Morphophysiology and ultrastructure of the male reproductive accessory glands of the bats Carollia perspicillata, Glossophaga soricina and Phyllostomus discolor (Chiroptera: Phyllostomidae), Acta Histochemica, 10.1016/j.acthis.2016.07.005, 118, 6, (640-651), (2016).
- 91.Fernandez D.S., Ferraz R.H.S., Melo A.P.F., Rodrigues R.F., Souza W.M. (2010). Análise histológica das glandulas uretrais da capivara (Hydrochoerus hydrochaeris) // Pesq. Vet. Bras. 30(4): 373–378.
- 92.Fernando Leis-Filho A.; Fonseca-Alves C.E. Anatomy, Histology, and Physiology of the Canine Prostate Gland. Vet. Anat. Physiol. 2018. In book: Veterinary Anatomy and Physiology (pp.1-14).
- 93.Frandson D.R., Wilke L.W., Fails D.A. Anatomy and Physiology of Farm Animals. Wiley Blackwell Ames Iowa Hearing and Balance. 2009: 192–194.
- 94.Garcia P.J., Cagnon V.H.A., Mello W.Jr., Martinez M. and Martinez F.E. 1999. Ultrastructural observations of the dorsal lobe of the prostate of rats (Rattus norvegicus) submitted to experimental chronic alcohol ingestion // Rev. Chil. Anat., 17 153-159.
- 95. <u>Ginja M., Maria J. P., Gonzalo-Orden J.M., Seixas F., Correia-Cardoso M., Ferreira R., Fardilha M., Oliveira P. A., Faustino-Rocha A. I.</u> Anatomy and Imaging of Rat Prostate: Practical Monitoring in Experimental Cancer-Induced Protocols //

- Diagnostics (Basel). 2019. Jun 30; 9(3): 68. 2-16 doi: 10.3390/diagnostics9030068.
- 96.Gomes I.C., Cagnon V.H., Carvalho C.A., De Luca I.M. 2002. Stereology and ultrastructure of the seminal vesicle of C57/BL/6J mice following chronic alcohol ingestion // Tissue Cell, 34, 177–186.
- 97.Gofur M. Anatomy and histomorphometry of accessory reproductive glands of the Black Bengal buck // Eur. J. Anat. 2015; 19 (2): 171-178.
- 98.Grabowska M., DeGraff D., Yu X., Jin R., Chen Z., Borowsky A. (2014). Mouse models of prostate cancer: picking the best model for the question // Cancer Metastasis Rev. 46, 38-46
- 99.Hayashi N. Morphological and functional heterogeneity in the rat prostate gland / N. Hayashi, Y. Sugimura, J. Kawamura et al. // Biology of Reproduction. 1991. Vol. 45, № 2. P. 308-321.
- 100.Holst B. S., Carlin S., Fouriez-Lablée V. (2021) Concentrations of canine prostate specific esterase, CPSE, at baseline are associated with the relative size of the prostate at three-year follow-up BMC Veterinary Research, 14, 46-57. ISSN 1746-6148, E-ISSN 1746-6148, Vol. 17, no 1, article id 173.
- 101.Holtz W., Foote R.H. (1978). The anatomy of the reproductive system in male Dutch rabbits (Oryctolaguscuniculus) with special emphasis on the accessory sex glands // J. Morphol. 158:1–20.
- 102. Ittmann M. Anatomy and Histology of the Human and Murine Prostate // Journal List Cold Spring Harb Perspect Med. 2018 v.8 (5). P.38-49.
- 103.Jan Philipp Radtke, Claudia Kesch, David Bonekamp, Imaging of the Large Prostate, The Big Prostate, 10.1007/978-3-319-64704-3, (23-40), (2018).
- 104.Jacob S., Poddar S. (1986). Morphology and histochemistry of the ferret prostate // Acta Anat 125: 268-273.

- 105.Jesik C.J., Holland J.M., Lee C. An anatomic and histologic study of the rat prostate // Prostate. 3 (1982) 81–97. doi:10.1002/pros.2990030111.
- 106.Joon Hyuk Sohn, Dai Fukui, Taro Nojiri, Kazuhiro Minowa, Junpei Kimura, Daisuke Koyabu, Three-Dimensional and Histological Observations on Male Genital Organs of Greater Horseshoe Bat, Rhinolophus ferrumequinum // Journal of Mammalian Evolution, 10.1007/s10914-020-09525-6, 28, 2, (559-571), (2020).
- 107.Key Pinheiro P.F.F., Almeida C.C.D., Segatelli T.M., Martinez M., Padovani C.R., Martinez F.E. (2003) Structure of the pelvic and penile urethrarelationship with the ducts of the sex accessory glands of the Mongolian gerbil (Meriones unguiculatus) // J. Anat. 202: 431–444.
- 108.Kheddache A., Moudilou E. N., Zatra Y., Aknoun-Sail N., Amirat Z., Exbrayat J., Khammar F. Seasonal morphophysiological variations in the prostatic complex of the Tarabul's gerbil (Gerbillus tarabuli) // Tissue and Cell, 10.1016 /j.tice.2017.01.004, 49, 2, (345-357), (2017).
- 109.Klassen W.R., Persaud N.V.T. 1978. Influence of alcohol on the reproductive system on the male rat // Int. J. Fertil., 23, 176-184
- 110.Knoblaugh S., True L. 2011. Male reproductive system. In Comparative anatomy histology. A mouse and human atlas (ed. Treuting P, et al.), pp. 295–303. Elsevier, Amsterdam.
- 111.Knoblaugh S., Tretiakova M., Hukkanen R. Male reproductive system. In Comparative Anatomy and Histology: A Mouse, Rat and Human Atlas; Treuting, P., Dintzis, S., Montine, K., Eds.; Academic Press: Cambridge, MA, USA, 2017; pp. 335–338.
- 112.König H.E., Liebich H-G. (2013) Veterinary Anatomy of Domestic Mammals: Textbook and Colour Atlas. Schattauer Verlag, Stuttgart.- p. 235

- 113.Korzerzer R.M., Oladele S. B., Suleiman M.H. and Hambolu J.O. Macro-Anatomy of Male Reproductive Organs of African Striped Ground Squirrel (Xerus Erythropus) // Journal of Veterinary and Biomedical Sciences. Vol. 2 (1). PP 137 144, December, 2019. DOI: 10.36108/jvbs/9102.20.0161.
- 114. Kundu P. Anatomical studies on the accessory male sex glands (gross and microscopic) of the Indian goat (Jamunapari and cross Jamunapari) // IJAH. 1980; 19 (2): 151-153.
- 115.Leroy B. E., Northrup N. (2009). Prostate cancer in dogs: Comparative and clinical aspects // Veterinary Journal, 180(2), 149–162.
- 116.Luce M.C., Coffey D.S. (1994) The male sex accessory tissues. KNOBIL E, NELLY JD (eds) In The Physiology of Reproduction. Raven Press: New York. pp: 1435-1489.
- 117. Mangera A., Osman N. I., Chapple C. R. (2013). Anatomy of the lower urinary tract (pp. 319–325). Elsevier Ltd.
- 118. Magri V., Boltri M., Cai T., Colombo R., Cuzzocrea S., De Visschere P.et al. Multidisciplinary approach to prostatitis // Arch. Ital. Urol. Androl. 2019; 90 (4): 227-248.
- 119. Martinez F.E., Garcia P.J., Padovani C.R., Cagnon V.H.A. and Martinez, M. 1993. Ultrastructural study of the ventral lobe of the prostate of rats submitted to experimental chronic alcoholism. Prostate, 22, 317-324.
- 120.Marker P., Donjacour A., Dahiya R., Cunha G. (2003). Hormonal, cellular, and molecular control of prostatic development // Dev Biol. 14, 28-37.
- 121. <u>Mateus R. Beguelini, Cintia C. I. Puga, Eliana Morielle-Versute, Sebastiao R. Taboga</u> Comparative analysis of the male reproductive accessory glands of bats Noctilio albiventris (Noctilionidae) and Rhynchonycteris naso (Emballonuridae) // J.Morphologi 2016, <u>Volume 277</u>, <u>Issue 11</u>, Pages 1459- 1468

- 122. McCracken T.H., Kainer R., Carlson D. (2008). Color Atlas of Small Animal Anatomy: The Essentials. Blackwell Publishing, USA, 72.
- 123. McNeal J.E. The zonal anatomy of the prostate // The Prostate. <u>Vol. 2</u>, <u>Issue 1</u>, 1981, Pages 35-49.
- 124. McNeal J.E., 1983. Relationship of the origin of benign prostatic hypertrophy to prostatic structure of man and other mammals. In: F. Hinman, editor. Benign prostatic hypertrophy. New York: Springer-Verlag. p. 152–166.
- 125. Mendes L.O. Mast cells and ethanol consumption: interactions in the prostate, epididymis and testis of UChB rats // L.O. Mendes, J.P. Amorim, G.R. Teixeira et al. // American Journal of Reproduction Immunology. -2011.-Vol. 66, Nolem 3. -P. 170-178.
- 126.Menezes D.J., Assis Neto A.C., Oliveira M.F., Farias E.C. (2010) Morphology of the male agouti accessory genital glands (Dasyprocta prymnolopha Wagler, 1831) // Pesq. Vet. Bras. 30: 793-797.
- 127.Michael Mitterberger, Wolfgang Horninger, Friedrich Aigner, Germar M. Pinggera, Ilona Steppan, Peter Rehder, and Ferdinand Frauscher. Ultrasonic imaging of prostate lesions. Cancer Imaging, 10(1): 30–48, 2019.
- 128.Miotti M.D., Mollerach M.I., Barquez R.M. (2018) Anatomy and histology of the prostate and glands of Cowper in three species of Neotropical bats // J. Morphol. 279: 294–301.
- 129.Moura F., Sampaio L., Kobayashi P., Laufer-Amorim R., Ferreira J.C., Watanabe T.T.N., Fonseca-Alves C.E. Structural and Ultrastructural Morphological Evaluation of Giant Anteater (Myrmecophaga tridactyla) Prostate Gland // Biology 2021, 10, 231-242.
- 130. Nascimento-Gonçalves E., Faustino-Rocha A.I., Seixas F., Ginja M., Colaço B., Ferreira R., Fardilha M., Oliveira P.A. Modelling human prostate cancer: Rat models // Life Sci. 2018, 203, 210–224.

- 131. Niu Y. J., Ma T. X., Zhang J., Xu Y., Han R. F., and Sun G., 2003: Androgen and prostatic stroma // Asian J. Androl. 5, 19–26.
- 132. Nicholson T.M., Ricke E.A., Marker P.C., Miano J.M., Mayer R.D., Timms B.G., vom Saal F.S., Wood R.W., Ricke W.A. (2012) Testosterone and 17 beta- estradiol induce glandular prostatic growth, bladder outlet obstruction, and voiding dysfunction in male mice // Endocrinology 153: 5556–5565.
- 133. Noguchi M., Stamey T., Neal J., Yemoto C. (2000). An analysis of 148 consecutive transition zone cancers:clinical and histological characteristics // J. Urol. 14: 48-57.
- 134.Oliveira D.S., Dzinic S., Bonfil A.I., Saliganan A.D., Sheng S., Bonfil R.D. Bosn. <u>The</u> mouse prostate: a basic anatomical and histological guideline // J. Basic Med. Sci. 2016 Feb 10; 16 (1): 8-13. doi: 10. 17305 /bjbms. 2016. 917. PMID: 26773172.
- 135.Oliveira C., Ferreira A.L. 1987. Effect of alcohol on the rat justa prostatic pelvic ganglia and gonads // Gegenbaurus Morphol. Jahrb., 133, 771-780.
- 136.Paner G. 2010. Prostate gland and seminal vesicle. In Diagnostic pathology: Genitourinary (ed. Amin M, et al.), Section 3, pp. 4–156. Amirysis, Salt Lake City, UT.
- 137.Pathak A., Katiyar R., Sharma D., Farooqui M., Prakash A. Gross anatomical, histological and histochemical studies on the postnatal development of the prostate gland of Gaddi goat // Int. j. morphol. 2012; 30 (2): 731-739.
- 138.Perez W., Vazquez N., Ungerfeld R. Gross anatomy of the male genital organs of the pampas deer (Ozotoceros bezoarticus, Linnaeus 1758) // Anat Sci Int. 2013; 88 (3):123-129.
- 139.Pierfrancesco Bo, Claudio Tagliavia, Marco Canova, Margherita De Silva, Cristiano Bombardi, Annamaria Grandis, Comparative characterization of the

- prostate gland in intact, and surgically and chemically neutered ferrets // Journal of Exotic Pet Medicine, 10.1053/j.jepm.2019.07.013, 78-84 (2019).
- 140.Prins G.S., Lindgren M. (2015) Accessory sex glands in the male // Knobil Neill's Physiol. Reprod. 1: 773–804.
- 141.Price D. 1963. Comparative aspects of development and structure in the prostate // Natl Cancer Inst. Monogr. 12: 1–27.
- 142.Ratcliffe F. 1972. The effect of chronic ethanol administration on the growth of rats // Arch. Int. Pharmacodyn., 197, 19-26.
- 143.Renata T. S. Santos, Laís R. M. Pires, Edna S. S. Albernaz, Cleber S. Andrade, Cornelio S. Santiago, Eliana Morielle Versute, Sebastiao R. Taboga, Mateus R. Beguelini. Morphological analysis of the male reproductive accessory glands of the bat Artibeus lituratus (Phyllostomidae: Chiroptera) // Journal of Morphology, 10.1002/jmor.20767, 279, 2, (228-241), (2017).
- 144.Riede U.N., Werner M. Allgemeine und Spezielle Pathologie, DOI 10.1007/978-3-662-48725-9_52, © Springer-Verlag GmbH Deutschland, 2017: 58.
- 145.Rivier C., Vale W. 1983. Influence of ethanol on reproductive junctions of the adult male as junction of body weight // Alcohol. Clin. Res., 7, 210-211.
- 146.Rowen D. Frandson, W. Lee Wilke, Anna Dee Fails. (2022) Anatomy and Physiology of Farm Animals SEVENTH EDITION, A John Wiley & Sons, Inc., Publication, 536 p.
- 147.Rochel S.S., Bruni-Cardoso A., Taboga S.R., Vilamaior P.S.L., Goes R.M. (2007) Lobe identity in the Mongolian gerbil prostatic complex: a new rodent model for prostate study // Anat Rec 290:1233–1247.
- 148.Rocco A., Compare D., Angrisani D., Sanduzzi Zamparelli M., Nardone G. Alcoholic disease: liver and beyond // World J. Gastroenterol. 2014; 20 (40): 146-529.

- 149.Roy-Burman Wu H., Powell W.C., Hagencord J., Cohen M.B. Genetically defined mouse models that mimic natural aspects of human prostate cancer development // Endocr Relat Cancer. 2004 Jun; 11(2): 225-254. doi: 10. 1677/erc. 0.01 10225.
- 150.Ruetten H., Cole C., Wehber M., Wegner K.A., Girardi N.M. (2020) An immunehisto chemical prostate cell identification key indicates that aging shifts procollagen 1A1 production from myofibroblasts to fibroblasts in dogs prone to prostate-related urinary dysfunction. PLOS ONE 15(7): 232-264.
- 151.Salonen I., Huhtaniemi I. 1990. Effects of chronic ethanol diet on pituitary-testicular function of the rat // Biol. Reprod., 42, 55-62.
- 152.Santamaría L., Ingelmo I., Alonso L., Pozuelo J., Rodriguez R. The prostate of the rat. In Neuroendocrine Cells and Peptidergic Innervation in Human and Rat Prostate; Springer: Berlin/Heidelberg, Germany, 2007; pp. 39–42.
- 153.Sattolo S., Carvalho C.A.F., Cagnon V.H.A., 2004. Influence of hormonal replacement on the ventral lobe of the prostate of rats (Rattus norvegicus albinus) submitted to chronic ethanol treatment // Tissue Cell. 36, 417–430.
- 154.Singh B. (2017) Dyce, Sack and Wensing's Textbook of Veterinary Anatomy, 5th edn. Elsevier Health Sciences, London Smith JD (1976) Chiropteran evolution. In: Baker R.J., Jones J.K., Carter D.C. (eds) Biology of Bats of the New World Family Phylostomidae, Part I. Special Publication of the Museum of Texas Technical University, Lubbock, pp 49–69.
- 155.Smith J. Canine prostatic disease: A review of anatomy, pathology, diagnosis, and treatment. Theriogenology. 2008; 70: 375-383. DOI: 10. 1016 /j. therio geno logy. 2008.04.039.
- 156.Stan F. Anatomical Particularities of Male Reproductive System of Guinea Pigs (Cavia porcellus) // Bulletin UASVM Veterinary Medicine 72(2) / 2015, 288-

- 295 Print ISSN 1843-5270; Electronic ISSN 1843-5378 DOI:10.15835/buasvmcn-vm: 11410.
- 157.Sugimura Y., Cunha G.R., Donjacour A.A. 1986. Morphogenesis of ductal networks in the mouse prostate // Biol Reprod 34: 961–971.
- 158.Symons M.A., Marks V. 1975. The effects of alcohol on weight gain and the hypothalamic-pituitary-gonadotrophin axis in the maturing male rat // Biochem. Pharmacol., 24, 955-958.
- 159.Shappell S.B., Thomas G.V., Roberts R.L., Herbert R., Ittmann M.M., Rubin M.A., Humphrey P.A., Sundberg J.P., Rozengurt N., Barrios R., Ward J.M., Cardiff R.D. 2004. Prostate pathology of genetically engineered mice: definitions and classification. The consensus report from the Bar Harbor meeting of the Mouse Models of Human Cancer Consortium Prostate Pathology Committee // Cancer Res. 64: 2270- 2305.
- 160.Shirai T., Takahashi S., Cui L., Futakuchi M., Kato K., Tamano S., Imaida K. Experimental prostate carcinogenesis Rodent models, Mutat. Res. Rev. Mutat. Res. 462 (2000) 219–226. doi:10.1016/S1383-5742(00)00039-9.
- 161.Shirai T. Significance of chemoprevention for prostate cancer development: Experimental in vivo approaches to chemoprevention // Pathol. Int. 2007, 58, 1–16.
- 162.Schwartz E., Xie A., La J., Gebhart G. (2015). Nociceptive and inflammatory mediator upregulation in a mouse model of chronic prostatitis // Pain. -14: 78-86.
- 163.Takis A. Impact of hypercholesterol diet (HD) on the antioxidant system of the rat ventral prostate / A. Takis, A. Kyroudi-Voulgari, K. Ploumidou et al. // European Urology. 2009. Vol. 8, № 4. P. 208.
- 164.Timms B.G. Prostate development: A historical perspective, Differentiation. 76 (2008) 565–577. doi:10.1111/j.1432-0436.2008.00278.

- 165. Toivanen R., Shen M.M. Prostate organogenesis: Tissue induction, hormonal regulation and cell type specification // Development. 2017; 144: 1382–1398. doi: 10.1242/dev.148270.
- 166.Tsonis C.G., Gaughwin M.D., Breed W.G. 1981. Biochemistry of male accessory organs of conilurine rodents // Arch. Androl. 6: 239–242.
- 167. Vasquez B., Del Sol M. (2002). Complejo prostatico en el conejo (Oryctolaguscuniculus) // Rev Chil. Anat. 20: 175-180.
- 168. Vezina C.M., Bushman A.W. (2015). Hedgehog signaling in prostate growth and benign prostate hyperplasia // Curr. Urol. Rep. 8: 275–280.
- 169. Vickman R. E., Franco O. E., Moline D. C., Vander Griend D. J., Thumbikat P., & Hayward S. W. (2019). The role of the androgen receptor in prostate development and benign prostatic hyperplasia: A review. Editorial Office of Asian Journal of Urology, 7: 191–202.
- 170.Watanabe H. et al. Ultrasonographi of the prostate (2 nd report): sagittal tomographi of the prostate using B-scope scanning // Jpn. J. Ultrasound Med. -1974. Vol.141. P.233-239.
- 171.Whitney K. Male accessory sex glands. In Boorman's Pathology of the Rat: Reference and Atlas; Suttie A., Leininger J., Bradley A., Eds.; Academic Press Elsevier: Cambridge, MA, USA, 2018; pp. 579–586.
- 172.Willis B.R., Anderson Jr. R.A. Oswald, C. and Zaneveld L.J.D. 1983. Ethanol-induced male reproductive tract pathology as a function of ethanol dose and duration of exposure // J. Pharmacol. Exp. Ther., 225, 470-478.
- 173.William A. Ricke, Barry G. Timms, Frederick S. vom Saal, Prostate Structure, Encyclopedia of Reproduction, 10.1016/B978-0-12-801238-3.64596-8, (315-324), (2018).

174.Wrobel K. H., and Bergmann M. 2006: Male reproductive system. In: Dellman's Textbook of Histology, 6th edn. (J. A. Eurell, and B. L. Frappier, eds). Iowa: Blackwell Publishing Ltd. pp. 233–255.

175.Yassa H.A. Subchronic toxity of cannabis leaves on male albino rats /H.A. Yassa, W. Dawood Ael, M.M. Shehata et al. // Human & Experimental Toxicology. – 2010. – Vol. 29, № 1. – P. 37-47.

176.Zyryanov A.V., Surikov A. S., Ponomarev A. V., Keln A. A., Znobishchev V. G., Prostate volume as an independent predictor of results robot-assisted prostatectomy // Cancer Urology, 10.17650/1726-9776-2019-15-4-73-83, 15, 4, (73-83), (2020).